

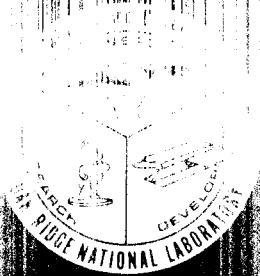
LOCKHEED MARTIN ENERGY RESEARCH LIBRARIES



3 4456 0515186 7

ORNL-5089

cy 1



Metals and Ceramics Division Materials Science Annual Progress Report for Period Ending June 30, 1975

OAK RIDGE NATIONAL LABORATORY
CENTRAL RESEARCH LIBRARY
DOCUMENT COLLECTION

LIBRARY LOAN COPY

DO NOT TRANSFER TO ANOTHER PERSON

If you wish someone else to see this
document, send in name with document
and the library will arrange a loan.

UCN-7463
(3-2-67)



OAK RIDGE NATIONAL LABORATORY

OPERATED BY UNION CARBIDE CORPORATION • FOR THE U.S. ATOMIC ENERGY COMMISSION

Printed in the United States of America. Available from
National Technical Information Service
U.S. Department of Commerce
5285 Port Royal Road, Springfield, Virginia 22161
Price: Printed Copy \$5.45; Microfiche \$2.25

This report was prepared as an account of work sponsored by the *United States* Government. Neither the United States nor the Energy Research and Development Administration, nor any of their employees, nor any of their contractors, subcontractors, or their employees, makes any warranty, express or implied, or assumes any legal liability or responsibility for the accuracy, completeness or usefulness of any information, apparatus, product or process disclosed, or represents that its use would not infringe privately owned rights.

ORNL-5089
UC-25 - Materials

Contract No. W-7405-eng-26

METALS AND CERAMICS DIVISION MATERIALS SCIENCE ANNUAL PROGRESS REPORT
FOR PERIOD ENDING JUNE 30, 1975

Compiled by C. J. McHargue, Manager, Materials Science

Edited by Sigfred Peterson

OCTOBER 1975

OAK RIDGE NATIONAL LABORATORY
Oak Ridge, Tennessee 37830
operated by
UNION CARBIDE CORPORATION
for the
U.S. ENERGY RESEARCH AND DEVELOPMENT ADMINISTRATION

LOCKHEED MARTIN ENERGY RESEARCH LIBRARIES



3 4456 0515186 7

FOREWORD

C. J. McHargue

Since most programs of the Metals and Ceramics Division report progress on a quarterly or semiannual schedule, the need for an annual report has diminished. However, work supported by the Office of Materials Science, Division of Physical Research is usually published in the open literature. In order to give a view of this program in the Metals and Ceramics Division an annual report has been prepared. It consists of abstracts of papers published or presented during the year ending June 30, 1975, and summaries of work in progress.

Following the reports of our technical progress is an Appendix listing (1) assignments of our staff in other organizations, (2) guest assignments in our section, (3) joint appointments of our staff with the University of Tennessee for the academic year 1974-1975, (4) papers presented at technical meetings, and (5) publications.

CONTENTS

SUMMARY	xi
1. STRUCTURE OF MATERIALS	1
1.1 THEORETICAL RESEARCH	1
1.1.1 Cluster Calculations of the Electronic Structure of Transition Metal Surfaces	1
1.1.2 Single-Site Numerical Orbitals for the Calculation of the Electronic Structure of Clusters	1
1.1.3 Soft X-Ray Emission and Absorption in Diamond . . .	2
1.1.4 Electronic Structure and Optical Properties of the 3C Form of Silicon Carbide	2
1.1.5 Electronic States of Substoichiometric PdH	2
1.1.6 Muffin-Tin CPA Calculations on a Model of a Transition Metal Alloy	2
1.1.7 On the Anderson-McMillan Prescription for the Density of States of Liquid Iron	3
1.1.8 Residue Normalization of KKR Eigenfunctions	3
1.1.9 Theory of the Optical Anisotropy of Homogeneous Pyrocarbons	4
1.1.10 Steady-State Diffusion of Point Defects in the Interaction Force Field	4
1.2 BASIC RESEARCH ON X-RAY DIFFRACTION	4
1.2.1 Intervariant Interference Effects in Partially Decomposed Alloys	5
1.2.2 Crystal Structure of Transition Metal Tellurides .	6
1.2.3 Computer Programs of General Use in X-Ray Crystallography	6
1.2.4 Excess Diffuse X-Ray Scattering and Anomalous Dispersion	7
1.2.5 X-Ray Diffraction and Fluorescence at the Stanford Synchrotron Radiation Project	8
1.2.6 Inelastic Resonance Emission of X Rays: Anomalous Scattering Associated with Anomalous Dispersion . .	8
1.2.7 Neutron Irradiation Effects and Structure of Noncrystalline SiO ₂	9
1.2.8 Studies of Voids in Neutron-Irradiated Aluminum Single Crystals I. Small-Angle X-Ray Scattering and Transmission Electron Microscopy	9

1.2.9	Studies of Voids in Neutron-Irradiated Aluminum Single Crystals II. Small-Angle Neutron Scattering	10
1.2.10	A New Small-Angle X-Ray Scattering Spectrometer Using a Rotating Anode Generator, Pin-Hole Collimation, and a Two-Dimensional Position-Sensitive Proportional Counter	10
1.2.11	Quantitative X-Ray Fluorescence Analysis Using Fundamental Parameters	11
1.2.12	Effects of Neutron Irradiation on the Long-Range Order and Superconducting Temperatures of Nb ₃ Sn . .	11
1.3	ALLOY STRUCTURE	12
1.3.1	Computer Simulation of Solid Solutions	12
1.3.2	The Nature of the Limitations of Second Law Determinations of Solution Thermodynamics	13
1.3.3	The Importance of Multiple X-Ray Scattering in Measurements of Diffuse Intensity	13
1.3.4	Flip-Flop Decomposition Within Miscibility Gaps . .	14
1.4	FUNDAMENTAL CERAMICS	14
1.4.1	Refractory Europium Compounds	14
1.4.2	Surface Properties of Europium Oxide: Initial Studies	14
1.4.3	Unidirectional Solidification of Eu ₂ O ₃ -Mo Composites	15
1.4.4	Thermodynamic and Chemical Properties of Transition Metal Tellurides	15
1.4.5	Crystallization of Eu ₂ O ₃ and Eu ₂ O ₃ -Containing Compounds From Molten-Salt Solvents in the Range 900-1400°C	15
1.5	CRYSTAL PHYSICS	16
1.5.1	Directional Solidification by Internal Zone Melting of Cr ₂ O ₃ -Mo Composites	16
1.5.2	Experimentally Scaling Up Internal Zone Growth . .	17
1.5.3	Mathematical Modeling of Internal Zone Growth . . .	17
1.5.4	The Directional Solidification of Pb-Sn-Cd Alloys .	18
1.5.5	Unidirectional Solidification of a MnO-Mn ₂ SiO ₄ Eutectic by the Edge-Defined Film-Fed Method . . .	18
1.5.6	Effect of Temperature on the Self-Luminescence of SrCl ₂ Doped with ²⁴⁴ Cm or ²⁵³ Es: Observation of Host Defect Emission	19

1.5.7	Growth of Single-Crystal Mn_2SiO_4 (Tephroite) by Czochralski and Edge-Defined, Film-Fed Techniques .	19
1.5.8	EPR Investigations of $^{253}Es^{2+}$ in Single Crystals of BaF_2 and $SrCl_2$	20
1.5.9	Measurement of Q for RbOH-Grown Quartz	20
2.	DEFORMATION AND MECHANICAL PROPERTIES	23
2.1	AGING-INDUCED SHAPE INSTABILITY IN AN ELASTICALLY BENT U-7.5 wt % Nb-2.5 wt % Zr ALLOY; A REVERSE SHAPE MEMORY EFFECT	23
2.2	TRANSMISSION ELECTRON MICROSCOPY OF PROPENE-DERIVED PYROLYTIC CARBON	24
2.3	PRECIPITATION HARDENING IN ALUMINUM-GOLD ALLOYS	24
2.4	THE MICROSTRUCTURE OF COAL	25
3.	PHYSICAL PROPERTIES AND TRANSPORT PHENOMENA	27
3.1	PHYSICAL PROPERTIES RESEARCH	27
3.1.1	Lattice Thermal Conductivities in Electrically Insulating Crystals	27
3.1.2	Physical Properties of Metals	29
3.1.2.1	Chromium	29
3.1.2.2	Tungsten	29
3.1.2.3	Molybdenum	29
3.1.2.4	Aluminum	30
3.1.2.5	Nickel-Base Alloys	30
3.1.2.6	Specific Heat of ^{241}Am and $PuC_{0.8}$	31
3.1.3	Apparatus Development	31
3.1.3.1	Thermal Expansion Apparatus	31
3.1.3.2	CODAS Development	32
3.2	SURFACE PHENOMENA	32
3.2.1	Oxidation of Uranium-Base Alloys	33
3.2.1.1	Current Investigations	33
3.2.1.2	The Development of Product Microstructures During the Diffusion-Controlled Oxidation of Uranium Alloys	33
3.2.1.3	Mechanisms of Stress Generation and Relaxation During the Oxidation of Uranium Alloys	34

3.2.2	Refractory Metal Alloys	34
3.2.2.1	Current Research	34
3.2.2.2	Some Oxidation Characteristics of Ta-10% W and Ta-10% W-2.5% Hf Alloys	35
3.2.3	Computer Code Development	35
3.2.4	Ceramic-Metal Composites	35
3.3	DIFFUSION IN SOLIDS	36
3.3.1	Interdiffusion and Vacancy Wind Effects	36
3.3.1.1	Current Investigations	36
3.3.1.2	MANTANØ - A Computer Code for the Analysis of Interdiffusion and Intrinsic Diffusion Information in Binary Systems	37
3.3.1.3	Interdiffusion and Intrinsic Diffusion in Binary Vanadium-Titanium Solid Solutions at 1350°C	37
3.3.1.4	Atomic Mobilities and Vacancy Wind Effects for Diffusion in Ternary Silver-Zinc- Cadmium Solid Solutions	38
3.3.2	Interstitial Diffusion	39
3.4	SUPERCONDUCTING MATERIALS	39
3.4.1	A Comparison of Methods for Measuring Flux Gradients in Type II Superconductors	39
3.4.2	The Effects of Yttrium or Gadolinium on the Super- conducting Transition Temperature of Niobium	40
3.4.3	Critical Temperature and Its Pressure Dependence for Technetium-Base HCP Solid-Solution Alloys	40
3.4.4	Superconductivity in the Technetium-Titanium Alloy System	41
3.4.5	A Study of the Frequency Dependence of AC Losses in Type II Superconductors	41
3.4.6	Work in Progress and in Support of Other Programs	42
4.	RADIATION EFFECTS	43
4.1	THEORY	43
4.1.1	Diffusion of Point Defects in Irradiated Metals	43
4.1.2	Point Defect Diffusion Bias for Finite Dislocation Loops	44
4.1.3	The Climb of Edge Dislocations During Irradiation	44

4.1.4	Prediction of Irradiation Creep From Microstructural Data	46
4.1.5	Comparison of Void Growth Kinetics in Irradiated Stainless Steels and Pure Metals	49
4.2	NEUTRON DAMAGE	51
4.2.1	Void Nucleation as Inferred from Neutron Irradiations	51
4.2.2	The Influence of Implanted Helium on the Development of Damage Structure in Neutron-Irradiated Aluminum	52
4.2.3	The Effects of Solute Content and Precipitate Distribution on Fast-Neutron Damage in Aluminum-Copper Alloys	53
4.2.4	Synergistic Effects of Displacement Damage and High Gas Content in Aluminum	53
4.2.5	Neutron Damage in Zirconium	54
4.3	DAMAGE SIMULATION	54
4.3.1	Improvements to the ORNL Heavy-Ion Bombardment Facility	54
4.3.2	A Method for Doping Irradiation Samples with Helium Using ^{244}Cm	55
4.3.3	Current Nickel Ion Bombardment Experiments	56
4.3.4	The ORNL Irradiation Creep Facility	57
4.3.5	The ORNL High-Voltage Electron Microscope Facility	57
APPENDIX	59

SUMMARY

1. STRUCTURE OF MATERIALS

Multiple scattering cluster programs have been developed and applied to a range of problems such as calculation of charge distributions on both flat and stepped surfaces of transition metals. The bonding orbitals found on stepped surfaces are of interest in catalysis. A new technique for cluster calculations has been developed that doesn't require the muffin-tin approximation.

The discrete variational method that we developed for band theory calculations on covalent materials has been used to calculate the soft x-ray emission and absorption in diamond and the optical properties of the 3C form of SiC.

The coherent potential approximation (CPA) has been used as a basis for a new theory of the electronic states in nonstoichiometric crystals that have vacancies on the anion sites. A critical comparison of the CPA with other theories for substitutive alloys had led to a better understanding of the approximation. The widely quoted Anderson-McMillan theory for liquid metals has been shown to be wrong.

Combining our work on band theory, multiple scattering theory, and Green's functions, substantial improvements in our constant-energy KKR band theory techniques have been developed. This tool is presently being used to obtain the Fermi surfaces, densities of states, and wave functions for elements 37 through 47 and to calculate the critical temperature of these elements for superconductivity.

A theory of the optical anisotropy of pyrocarbons has been developed.

The diffusion equation, including the drift term due to the long-range interaction between the point defect and a spherical sink, is solved by use of a technique we developed.

Progress in x-ray diffraction research includes completion of small-angle scattering studies on neutron-irradiated aluminum and SiO₂. Results are consistent with and supplement data from other experiments — such as transmission electron microscopy, small-angle neutron scattering, and Raman spectroscopy — performed on the same samples. Details of the faceting of void surfaces in irradiated aluminum have been deduced for the first time.

We have augmented our model of short-range "omega" structures to include all intervariant interference effects in the total predicted scattered intensity distribution. The theoretical maps are accurate for any given short-range structure model based on specified laws of probability governing the sequences of atom configurations.

A new inelastic resonance x-ray emission process is reported. Its existence may explain certain inconsistencies in elastic diffuse scattering measurements from short-range-ordered alloys. The observed effect is correlated with the real part of the well-known anomalous dispersion corrections to elastic scattering cross sections.

The status of our continuing structural studies of transition metal tellurides is reviewed. Data for a new ternary telluride, NiTiTe₂, are presented.

Experiments designed to assess the utility of synchrotron x radiation in diffraction and fluorescence analyses were performed. Order-of-magnitude estimates of the intensity and angular resolution of the synchrotron source relative to conventional x-ray generators demonstrate the potential advantages of synchrotron radiation and serve to stimulate the search for areas in atomic physics and materials science research to which it may be applied.

The effect of multiple scattering on diffuse x-ray scattering by alloys was investigated. Two cases were considered: a diffusely scattered beam subjected to Bragg scattering and a Bragg-scattered beam subsequently diffusely scattered before emergence from a specimen. The efficiency of a computer program designed to simulate diffuse scattering by alloys was greatly improved. The nature of solid-solution alloys was also investigated through an examination of the problems associated with deriving entropy and heat of mixing values solely from free energy measurements.

Basic properties of refractory europium compounds are being studied, with focus on potential applications as LMFBR neutron absorbers. Phase relationships and thermodynamic properties of transition metal tellurides are being studied, with emphasis on the intergranular attack of tellurium in nickel-base alloys.

Using our internal zone growth technique, we have grown dendrite-free, rod-type off-eutectic composites of Cr_2O_3 -28, -35, and -40 mole % Mo. Rigorous thermomechanical calculations were used to predict the optimum oxygen pressure and choice of gases for these experiments. We have scaled up our technique of directional solidification by internal zone melting so as to produce melt-zone areas 2.5 times larger with a power increase of only 60%. We are collaborating with some of the staff of Carnegie-Mellon University to test experimentally their mathematical modeling of internal zone growth. To provide a better understanding of heat flow, thin film, capillary, and die geometry effects in the edge-defined, film-fed growth technique, we have grown and analyzed cylindrical samples of off-eutectic $\text{MnO-Mn}_2\text{SiO}_4$. Unexpected rod discontinuities on a plane parallel to the solid-liquid interface (banding) have been observed at slow growth rates and are believed to be caused by a periodic fluctuation in interface location and/or by non-steady-state diffusion fields in the liquid film. The temperature dependence of self-luminescence in the wavelength range 300 to 700 nm has been studied on our SrCl_2 crystals doped with ^{244}Cm or ^{253}Es . Optically transparent single crystals of Mn_2SiO_4 (tephroite) were grown by the Czochralski and edge-defined, film-fed methods. EPR investigations of $^{253}\text{Es}^{2+}$ in single crystals of BaF_2 and SrCl_2 are reported. Recently we grew from the solvent 0.5 *N* RbOH a crystal of quartz of sufficient size to permit the direct measurement of both Q and $\alpha(3500\text{ cm}^{-1})$. A plot of this single data point does not fall on published curves relating Q and $\alpha(3500\text{ cm}^{-1})$ for synthetic quartz grown either from NaOH or Na_2CO_3 . These data may reflect a higher degree of intrinsic perfection of Rb^+ -grown quartz. We are now constructing a larger autoclave system so as to grow larger crystals and evaluate this possibility.

2. DEFORMATION AND MECHANICAL PROPERTIES

Reverse shape memory effects in a metastable U-7.5 wt % Nb-2.5 wt % Zr alloy were shown to result from the interplay between the deformation mechanism of mechanical twinning, the development of preferred orientations, and the low-temperature aging of the alloy. The growth features and microstructures of propene-derived pyrocarbon coatings were examined and characterized by transmission electron microscopy. The nature of the coating depended on the deposition temperature. High residual resistivity ratios were produced in precipitation-hardenable aluminum-gold alloys.

3. PHYSICAL PROPERTIES AND TRANSPORT PHENOMENA

Thermal conductivity of CsCl was measured and compared with previous results on the rubidium-halides. The thermal conductivities of KCl and two KCl alloys were calculated and compared with recent experimental results by others. The Lorenz number and lattice conductivity values for molybdenum and some dilute alloys were determined with measurements on Mo-Nb and Mo-Zr alloys. Transport properties of two nickel-base alloys of potential use as thermoelements were measured. The specific heats of ^{241}Am and $\text{PuC}_{0.8}$ were measured. Work continued on techniques to obtain more accurate physical property results on solids. This included development of a "plane probe" technique for measurements on salts and tests for reducing the time required for making CODAS-operated measurements of thermal expansion.

We continued our investigations of the effect of alloying elements on the defect diffusion coefficients and concentrations in oxide scales on alloys. The relationship between oxide morphology and the relative rates of diffusion in an oxide scale and the substrate alloy was studied for systems in which anion diffusion predominates in the oxide. Oxidation and diffusion phenomena in several tantalum and niobium-base alloys were characterized, and the reactions of urania-tungsten composites in low-pressure oxygen, CO-CO₂ mixtures, and methane were investigated.

Interdiffusion, intrinsic diffusion, and vacancy wind effects were studied for a series of V-Ti alloys, and a computer program for calculating these quantities from experimental data was developed. Similar work with the ternary system V-Ti-Cr was initiated. We also began studies of interstitial diffusion processes for tritium diffusion in CoO and oxygen in niobium alloys.

We compared four methods of measuring superconducting critical current density in selected materials with varying superconducting properties. The influence of small amounts of yttrium or gadolinium on the superconducting transition temperature of niobium was studied. The superconducting transition temperature and its pressure dependence were determined for a number of technetium-base hcp solid-solution alloys. We surveyed superconducting transition temperatures and crystal structures for the technetium-titanium alloy system. The frequency dependence of ac losses was studied in representative type II superconductors. Work in progress on fluxoid pinning in Nb-Hf and Nb-Ti alloys is presented as well as work in support of stress effects on commercial superconductors.

4. RADIATION EFFECTS

The Radiation Effects Program supported by the Division of Physical Research is directed at identifying the mechanisms responsible for changes in microstructure and mechanical properties during neutron irradiation. Its ultimate aim is to provide guidance for the development of improved materials for reactor applications. It includes a blend of theoretical and experimental tasks and relies heavily on damage simulation techniques.

Theoretical studies of diffusion of point defects to sinks during irradiation are described; these include calculations of bias factors and the rate of climb of edge dislocations. The latter is used to estimate irradiation creep behavior from knowledge of the microstructure. Void growth kinetics is shown to depend on whether the voids or dislocations are the predominant sink for point defects. Implications of the limiting cases are discussed.

General observations on the nucleation of voids during neutron irradiation and the conclusions that can be drawn from them are summarized. Experiments describing the role of helium on the nucleation of voids and dislocation loops are reported. Effects of solute concentration and precipitate distribution on swelling during neutron irradiation are described for aluminum-copper alloys. Some effects of very high neutronically generated gas contents on the swelling and mechanical properties of aluminum are given; severe embrittlement is seen even at low temperatures. The formation of cavities in zirconium during neutron irradiation is related to helium content. The cavities that are found are concluded to be helium bubbles of near-equilibrium size.

Modifications to the ORNL 5-MeV van de Graaff during the year have increased the intensity and uniformity of the heavy-ion beam used in damage simulation experiments. A simple technique for injecting uniform layers of helium into specimens before ion bombardment is described. Current experiments using the heavy-ion facility intend to assess swelling behavior of Fe-Cr-Ni alloys, to establish a correlation between ion and neutron irradiation, and to identify reproducible specimen preparation techniques. The light-ion bombardment facility for the study of irradiation creep is described. Design is nearly complete, and preliminary experiments show that the high level of temperature control required for the experiment can be obtained. The high-voltage electron microscope, which was upgraded to 1 MeV potential during the year, is now operational. Examination of dislocation loop formation is described.

1. STRUCTURE OF MATERIALS

1.1 THEORETICAL RESEARCH — J. S. Faulkner

We have contributed to the development of the anisotropic elasticity theory of dislocations, the Korringa-Kohn-Rostoker and discrete variational method approaches for calculating electronic states in ordered solids, the coherent potential approximation for obtaining the electronic states in disordered solids, and cluster methods for treating a range of problems in the theory of condensed matter. We are using these techniques to gain an understanding of the properties of technologically interesting materials in their normal states and after radiation damage.

1.1.1 Cluster Calculations of the Electronic Structure of Transition Metal Surfaces¹ — R. O. Jones,² P. J. Jennings,³ and G. S. Painter

The electronic structure and charge distributions for 13-atom clusters of 3d-transition metals (Fe, Ni, Cu) have been calculated by a scattered wave technique. The cluster geometry is chosen to display features of stepped and flat surfaces. Many states in the band show pronounced charge lobes in the neighborhood of edge and corner atoms, suggesting that these are active sites in these metals. These lobes are more extensive for lighter elements in the series and, for a given element, more diffuse at lower energies in the d-band. Charge expansion from the center of the cluster to the edge atoms is a general feature, and the stepped surfaces show a variety of bonding orbitals not present on the flat surface.

1.1.2 Single-Site Numerical Orbitals for the Calculation of the Electronic Structure of Clusters⁴ — G. S. Painter and G. M. Stocks⁵

A procedure is described for using separate atomic-like single-site potentials to define numerical basis sets for electronic structure calculations for clusters. A comparison of results is presented for the molecular eigenvalues of diatomic carbon treated with Slater-type orbitals and with a basis set of single-site orbitals. A calculation of the set of s-d levels for a cluster of two copper atoms is compared with the d-band density of states evaluated from the Lloyd cluster determinant.

¹Submitted for publication to the *Journal of Physics C*; presented at Warwick Surface Science Conference, Warwick, England, March 17-20, 1975.

²Institute of Physics, Fack, Göteborg, Sweden.

³University of New South Wales, Australia.

⁴To be published in *Solid State Communications*.

⁵Department of Physics, University of Bristol, England.

1.1.3 Soft X-Ray Emission and Absorption in Diamond⁶ - A. R. Lubinsky,⁷
D. E. Ellis,⁷ and G. S. Painter

The x-ray K-emission spectrum and the soft x-ray absorption spectrum are calculated for diamond and compared with experiment. The influence of transition matrix elements, calculated in a one-electron approximation, is discussed. Binding energy corrections on the core and valence states are estimated and used to explain differences between band transition energies and experimental data. Approximate methods are used to study localized valence relaxation effects on the transition matrix elements in emission.

1.1.4 Electronic Structure and Optical Properties of the 3C Form of Silicon Carbide⁶ - A. R. Lubinsky,⁷ D. E. Ellis,⁷ and G. S. Painter

The electronic energy bands and wavefunctions of cubic "3C"-SiC have been calculated in the first principles Hartree-Fock-Slater model, making use of the Discrete Variational Method. Experimental optical data, calculated indirect transitions, and theoretical results for $\epsilon_2(E)$ and reflectivity are compared. The valence band density of states is found to be in reasonably good agreement with x-ray emission spectra.

1.1.5 Electronic States of Substoichiometric PdH⁸ - J. S. Faulkner

A theory for the electronic states of substoichiometric compounds based on the coherent potential approximation was described previously. Using this theory extensive numerical calculations have been carried out on a model of PdH. The results and the applicability of the theory to this system and other systems are discussed.

1.1.6 Muffin-Tin CPA Calculations on a Model of a Transition Metal Alloy⁸ - William H. Butler

We have constructed a one-dimensional model of a transition metal alloy; the model includes the effects of resonant scattering. We have obtained the exact electronic density of states for the model and have compared it with the predictions of two approximate theories, the Coherent Potential Approximation (CPA) and the Average t -Matrix Approximation (ATA).

⁶Submitted for publication in *The Physical Review*.

⁷Department of Physics, Northwestern University, Evanston, Illinois.

⁸Abstract of a paper presented at the March Meeting of the American Physical Society, Denver, Colorado, March 31-April 3, 1975.

We have also compared the effective scattering amplitudes computed from the CPA and ATA. These calculations lead to the following conclusions, which can be shown to hold in three dimensions, as well as in one.

(1) The virtual bound state peak in the alloy density of states is shifted from its position for an isolated muffin tin. (2) The CPA generally predicts a more elastic effective scattering amplitude than the ATA away from resonant energies. (3) The density of states predicted by the CPA and ATA may be qualitatively similar even when there are appreciable differences in the CPA and ATA effective scattering amplitudes.

1.1.7 On the Anderson-McMillan Prescription for the Density of States of Liquid Iron⁶ - J. J. Olson

Our intensive numerical investigation has revealed a gross error in the density of states reported by Anderson and McMillan in their 1967 paper "Multiple Scattering Theory and Resonances in Transition Metals." Although they obtained a broad double-peaked resonance that appeared sufficiently reasonable to justify their prescription, correct evaluation of their formula yields a single structureless resonance far too narrow to be representative of a transition metal d -band. This conclusion was verified by algebraically reducing their expression for the density of states to a form that was easily evaluated by hand. Anderson and McMillan also erred in claiming that their dispersion relation led to a vanishing wave number at resonance. Their zero wave number, in fact, belongs on an extraneous branch and would have led to a nonintegrable singularity in their density of states. Evidently the Anderson-McMillan prescription is inadequate as a description of the effects of s - d hybridization on the density of states of transition metals.

1.1.8 Residue Normalization of KKR Eigenfunctions - J. J. Olson

Significant practical improvements in our KKR band theory programs have arisen as spin-offs from familiarity with the mathematical theory of Green's functions.

In the process of extending the KKR theory to calculate Green's functions we observed a simple connection between the residue of the Green's function and the normalization of the eigenfunctions. This connection has its basis in the k -dependence of the KKR determinant at a fixed energy and is therefore particularly well suited to the "constant energy search" technique pioneered by our group. By exploiting this connection we can now generate normalized eigenfunctions, the integrated density of states, and the density of states itself in essentially no more time than was previously required to calculate the constant-energy surfaces of the KKR band structure.

Another spin-off from the theory of Green's functions has allowed us to eliminate the so-called free electron singularities from the KKR determinant. This in turn has allowed the development of sophisticated new numerical search techniques, which have significantly increased the simplicity and reliability of our computer programs.

1.1.9 Theory of the Optical Anisotropy of Homogeneous Pyrocarbons –
J. J. Olson

Insofar as optical properties are concerned, a homogeneous pyrocarbon is equivalent to a polycrystalline graphite in which the microcrystallites are oriented stochastically according to some pole distribution function. We have shown that current theories relating the optical anisotropy to the pole distribution function are applicable only if the microcrystallites are much larger than the wavelength of light. However, x-ray measurements indicate that the microcrystallites are much smaller than the wavelength of light. In this limit the current theories are without physical foundation. We have outlined the salient physical principles that must be applied in this limit and have performed preliminary calculations relating the optical anisotropy to a particular moment of the pole distribution function.

1.1.10 Steady-State Diffusion of Point Defects in the Interaction Force Field⁹ – M. H. Yoo and W. H. Butler

The diffusion equation including the drift term due to the long-range interaction between a point defect and a spherical sink is solved numerically for the steady-state concentration of point defects. The effective capture radius of a sink is calculated from the flux integral of point defects, and the diffusion bias factors of an infinitesimal dislocation loop for interstitials and vacancies are obtained from the effective capture radii. Effects of temperature, point defect parameters, and elastic properties of the medium on the kinetics of vacancy-interstitial recombination and of point defect-dislocation loop growth are analyzed, and applications of the calculated results to the study of radiation-induced void formation are discussed.

1.2 BASIC RESEARCH ON X-RAY DIFFRACTION – H. L. Yakel

Our research interest is the measurement and interpretation of the patterns of scattered intensity that result from the irradiation of matter by x rays. In recent years important progress has been made in the technology used in experiments to measure such intensity patterns. X-ray sources of higher power and possibly different spectral content exist. Modern x-ray detectors are energy sensitive and may be capable of the simultaneous measurement of an intensity distribution along a line or in a plane. We are actively modifying experimental procedures and apparatus to exploit the new technology.

Any x-ray scattering pattern is composed of two parts: a coherent elastic diffraction pattern, which contains information concerning the

⁹Submitted for publication in *Acta Metallurgica*.

atomic arrangement, and an incoherent inelastic component resulting from the interaction of the radiation with the internal atomic structure. We are interested in both parts of the pattern.

1.2.1 Intervariant Interference Effects in Partially Decomposed Alloys — B. S. Borie and H. L. Yakel

A common phenomenon related to diffusionless solid-state transformations is the partial decomposition, upon quenching, of a high-temperature structure into one of lower symmetry with its orientation controlled by the high-temperature phase. Such systems that have recently been of interest to us include titanium- and zirconium-base alloys that partially transform to the hexagonal ω -phase and uranium-base alloys that upon rapid cooling form the tetragonal γ^S structure. In each case the high-temperature parent structure is bcc. For the ω phase, the cubic cell diagonal becomes the c axis of the low-temperature phase with no perceptible dimensional change relative to untransformed material. Since there are four equally likely choices for this cubic cell dimension, the partially transformed crystal will include regions associated with each of the four variants of the system in addition to untransformed regions. These five regions must presumably diffract coherently relative to each other. The decomposition of bcc into the γ^S configuration is such that a cubic cell edge becomes a tetragonal axis, and hence the system is characterized by three variants.

Our interest in these systems concerns the structural meaning of certain diffuse effects and diffraction maxima shifts observed for quenched samples, indicating that the transformed regions have grown with imperfections or faults. Models related to the nature of the faults have successfully reproduced most of the observed features of the intensity distribution in reciprocal space. However, the models used in our calculations have always included the assumption that the crystal contains only one variant and possibly untransformed material. Interference effects among the variants have been ignored.

We have now developed a theory to account for these effects. We previously reported its use to account for the interviant interference contributions to the sharp fundamental diffraction maxima, for which all variants and the untransformed regions have significant nonzero scattering amplitudes.¹⁰ However, since the transformed regions are defective, resulting in diffuse scattering, there may be other such regions of overlap giving rise to an interviant interference contribution to the diffuse scattering.

We have computed this component of the diffuse scattering for a partially transformed alloy of the ω phase. It is negative, it tends to be large in the vicinity of the fundamental maxima, and the magnitude of

¹⁰B. S. Borie and H. L. Yakel, "The Short-Range Structure of BCC Solid Solution Alloy of Titanium and of Zirconium," *Metals and Ceramics Div. Annu. Progr. Rep. June 30, 1974*, ORNL-4970, p. 7.

the effect appears to increase with distance from the origin in reciprocal space. This result allows us to find for the first time all components of the diffuse scattering related to a particular model.

1.2.2 Crystal Structure of Transition Metal Tellurides — H. L. Yakel

We have confirmed the reported^{11,12} monoclinic rickardite-type structure of Ni_3Te_2 .

A ternary nickel titanium telluride was prepared at ORNL by J. Brynstad by heating TiTe_2 with a nickel wire at 1050°C for several days. The crystal structure of this phase, NiTiTe_2 , has been determined from photographically recorded data. The unit cell is monoclinic C-centered, with $a_0 = 6.65 \pm 0.001 \text{ \AA}$, $b_0 = 3.835 \pm 0.005 \text{ \AA}$, $c_0 = 6.40 \pm 0.01 \text{ \AA}$, $\beta = 90.4 \pm 0.1^\circ$. With two formula weights of NiTiTe_2 per cell, the x-ray density is 7.38 g/cm^3 . The most probable space group is $C2/m$; atoms occupy the following special positions of this group:

2 Ni in $2a$: $0,0,0; 1/2,1/2,0$
 2 Ti in $2c$: $0,0,1/2; 1/2,1/2,1/2$
 4 Te in $4i$: $x,0,z$; etc., with $x \approx 1/3$ and $z = 3/4 + \delta$, with $\delta = 0.03 \pm 0.01$.

The structure is a monoclinic distortion of an ordered $\text{NiAs}(B8)$ -type¹³ arrangement.

1.2.3 Computer Programs of General Use in X-Ray Crystallography — H. L. Yakel

During the reporting period the following programs have been written or modified:

1. REGEL. — This FORTRAN IV program computes (a) Bragg angles and spacings for lattices with known dimensions, or (b) Bragg angles, spacings, and powder intensities for phases with known crystal structures. In the latter case, a CALCOMP or CRT plot of the powder pattern may be generated and/or saved for inclusion in a composite plot of patterns for several phases.

¹¹R. B. Kok, G. A. Wiegers, and F. Jellinek, "The System Nickel-Tellurium. I. Structure and Some Superstructures of the $\text{Ni}_{3\pm\alpha}\text{Te}_2$ Phase," *Rec. Trav. Chim. Pays-Bas* 84: 1585–88 (1965).

¹²J. Barstad et al., "On the Tellurides of Nickel," *Acta Chem. Scand.* 20: 2865–79 (1966).

¹³P. P. Ewald and C. Hermann, *Strukturbericht*, Band I, pp. 84–87, Akademische Verlagsgesellschaft m.b.H., Leipzig, 1931.

2. LAUEPL. — This FORTRAN IV program generates CRT plots of forward- or back-reflection Laue patterns from the superposition of up to four crystals with any specified orientations and crystallographic symmetries. The special designation of characteristic Laue reflections described by Christiansen, Gerward, and Alstrup¹⁴ has been incorporated in this program.

3. STEREO. — This program¹⁵ has been modified to the FORTRAN IV language.

1.2.4 Excess Diffuse X-Ray Scattering and Anomalous Dispersion¹⁶ —
C. J. Sparks, Jr.

Because the low cross sections for diffusely scattered x-rays may be comparable with those for other atomic processes, which may yield additional intensity, we have analyzed the energy of diffuse x-radiation to attempt to identify these possible components. Crystal-monochromated Cu K α or Mo K α radiation was scattered from various elements and alloys and analyzed with a Si(Li) solid-state detector. The observed intensities were placed on an absolute basis by comparison with the scattering from polystyrene. Corrections for polarization from the monochromator, dead time in the detector electronics, and double diffuse scattering were made to a previously listed value of the scattering from polystyrene. Fluorescence from both the sample and impurities in the sample is a possible source of extra intensity not necessarily removed by balance filters.

Another source of extra diffuse intensity is an inelastic scattering process, which differs from Compton scattering. The intensity of this radiation increases as the incident x-ray energy approaches an absorption edge and is independent of scattering angle. The intensity reaches a maximum at an energy lower than the incident energy by an amount equal to the binding energy of an inner shell electron. The cross section is predicted by summing the squares of the real part of the anomalous dispersion correction. We interpret these inelastically scattered x rays as arising from the resonance process associated with anomalous dispersion. This process can contribute significantly to measured diffuse intensities when the Hönl correction is large.

¹⁴G. Christiansen, L. Gerward, and I. Alstrup, "High-Precision Orientation of Crystals Using the Laue Method with Characteristic X-rays," *Acta Cryst.* A31: 142-45 (1975).

¹⁵H. L. Yake1, *Program STEREO: A FORTRAN-Language Program for Plotting Stereographic Projections of Lattice Plane Normals and Directions*, ORNL-TM-2461 (March 1969).

¹⁶Abstract of an invited paper presented at and to be published in the proceedings of the International Congress Conference on Anomalous Scattering, Madrid, Spain, April 22-26, 1974. This conference was sponsored by the International Union of Crystallography.

1.2.5 X-Ray Diffraction and Fluorescence at the Stanford Synchrotron Radiation Project^{17,18} - C. J. Sparks, Jr. and J. B. Hastings

Electrons circulating in synchrotrons and storage rings are an intense source of electromagnetic radiation of an energy from 1 eV to several keV. In March 1975, at the Stanford Synchrotron Radiation Project we performed experiments designed to evaluate and exploit the unique properties of this x-radiation source. Scattering of the broad x-radiation spectrum from polycrystalline materials produced powder diffraction patterns permitting compound identifications in less than 4 min, with the additional information of the fluorescent spectrum for elemental identification. The synchrotron operating at only 1.85 GeV and 8 mA gave 10 times more x-ray intensity in the 2 to 10 keV range than the continuous radiation spectrum from the highest powered commercially available x-ray sources. Scattering of this radiation from (111) planes of silicon single crystals gave diffraction peaks to the 11th order with excellent peak-to-background ratios. This resolution results from the small inherent divergence of the synchrotron radiation, which is 2×10^{-4} times that for radiation from conventional sources.

Fluorescence from trace impurities was measured at 90° to the incident beam in the plane of the synchrotron ring. Since the radiation from the synchrotron is plane polarized, coherent and Compton scattering should be minimal in this scattering direction. Results showed a hundredfold reduction in background under the fluorescence peaks, compared with the conventional x-ray fluorescence experiment, which uses unpolarized white radiation from a tungsten target. Double and higher multiple scattering processes were observed to occur with increasing probabilities as the average atomic number of the scattering material was decreased. The plane polarization of synchrotron x-radiation permits direct observation of higher order scattering processes, which were not previously measurable.

Brief experiments at higher synchrotron energies demonstrated the extremely high x-ray flux at energies of 2 to 25 keV available under these conditions; intensities that exceed the brehmsstrahlung from the most powerful conventional sources by a factor of 10^3 may be achieved, again with 5×10^3 better beam collimation.

1.2.6 Inelastic Resonance Emission of X Rays: Anomalous Scattering Associated with Anomalous Dispersion¹⁹ - C. J. Sparks, Jr.

An inelastic resonance scattering of monochromatic Cu $K\alpha$ x-rays incident on various targets is observed when an absorption edge of the

¹⁷This work was supported in part by the National Science Foundation Grant DMR73-07692 A02, in cooperation with the Stanford Linear Accelerator Center and the Energy Research and Development Administration.

¹⁸Abstract of oral presentation given at the Winter Meeting of the American Crystallographic Association, University of Virginia, Charlottesville, Va., March 9-13, 1975

¹⁹Abstracted from *Phys. Rev. Lett.* 33: 262-65 (1974).

target is just above the energy of the incident x-rays. This frequency-dependent and angular-independent inelastic scattering is interpreted with the x-ray scattering theory of anomalous dispersion. Conservation-of-intensity arguments allow a comparison of the observed inelastic intensity with the real part of the anomalous dispersion corrections to the coherent atomic scattering factors for x-rays.

This newly discovered scattering process will give additional information about the electronic nature of the atom. As a new spectrographic tool, it should open paths to greater understanding of the electronic effects so important to the physical and chemical properties of matter.

1.2.7 Neutron Irradiation Effects and Structure of Noncrystalline SiO₂²⁰ — J. B. Bates,²¹ R. W. Hendricks, and L. B. Shaffer²²

The nature of the defects produced in noncrystalline SiO₂ and α -quartz single crystals by fast-neutron irradiation (>0.18 MeV) has been investigated by Raman and infrared spectroscopy, small-angle x-ray scattering, and electron microscopy. Measurements were made at 25°C on samples irradiated to integrated fluxes (exposures) from about 1×10^{18} to 2×10^{20} n/cm². At 2×10^{20} n/cm², the α -quartz sample had been transformed to an essentially noncrystalline material. However, at 9×10^{19} n/cm², remnant crystallites of the original α -quartz having a radius of gyration of 47 Å were found. The spectra of the noncrystalline phase of these materials are interpreted in terms of local modes at defect centers. Simple models account for the vibrational spectra and extrapolated x-ray scattering in the forward direction. The postirradiation annealing behavior of the α -quartz samples has been followed to 1000°C. The structure of the noncrystalline phase gradually transformed to that of unirradiated SiO₂. In the α -quartz sample irradiated to 9×10^{19} n/cm², the remnant microcrystallites annealed out by 1000°C.

1.2.8 Studies of Voids in Neutron-Irradiated Aluminum Single Crystals
I. Small-Angle X-Ray Scattering and Transmission Electron
Microscopy²³ — J. E. Epperson,²⁴ R. W. Hendricks, and K. Farrell

Small-angle x-ray scattering and transmission electron microscopy experiments were performed on high-purity (99.9999+%) aluminum single crystals that had been neutron-irradiated to a fluence of 1.5×10^{21} n/cm² (>0.18 MeV) at 50°C. The volume changes determined by each technique are in good agreement. Evidence for scattering effects resulting from faceting

²⁰Abstract of paper published in *J. Chem. Phys.* 61: 4163–76 (1974).

²¹Solid State Division.

²²Visiting consultant from Anderson College, Anderson, Indiana.

²³Abstract of paper published in *Philos. Mag.* 30(4): 803–17 (1974).

²⁴Max Planck Institut für Metallforschung, Stuttgart, West Germany.

of the voids is presented. Assuming a truncated octahedral void shape, the ratios of the third to the second moment of the distribution of void sizes determined by both SAXS and TEM are in excellent agreement. The effects of isochronal annealing on the swelling have been followed to near the melting point. The annealing of voids was clearly seen; no evidence was found for bubble formation at elevated temperatures.

1.2.9 Studies of Voids in Neutron-Irradiated Aluminium Single Crystals
II. Small-Angle Neutron Scattering²⁵ — R. W. Hendricks,
 J. Schelten,²⁶ and W. Schmatz²⁶

Absolute small-angle neutron scattering measurements have been made on six aluminium single crystals irradiated with fast neutrons (>0.18 MeV) to fluences between 0.3 and 2.0×10^{21} n/cm². The results are interpreted in terms of the truncated octahedral shape of voids, and are compared with companion transmission electron microscopy and immersion density measurements. The swelling, total void surface area, radius of gyration, and the moment ratios of the size distribution ($\langle D^6 \rangle / \langle D^3 \rangle$ and $\langle D^3 \rangle / \langle D^2 \rangle$) are in good agreement. These quantities are not only fluence dependent but also show a marked temperature dependence resulting from the small thermal gradient in the reactor core.

1.2.10 A New Small-Angle X-Ray Scattering Spectrometer Using a Rotating Anode Generator, Pin-Hole Collimation, and a Two-Dimensional Position-Sensitive Proportional Counter — R. W. Hendricks

Previous experiments with a one-dimensional position-sensitive x-ray counter have indicated the feasibility of measuring various void size distribution parameters (radius of gyration, surface area, swelling, surface anisotropy) in very small (≈ 0.002 mm³) neutron-irradiated specimens by small-angle x-ray scattering.²⁷ To extend this technique to determine similar parameters for specimens in which the voids are created by heavy-ion damage, it was necessary to increase the detected x-ray intensity by approximately two orders of magnitude over our earlier system. To achieve this goal, we have constructed a new small-angle x-ray spectrometer, which features (1) a 5-m collimation distance and a 5-m specimen-to-detector distance, (2) a two-dimensional position-sensitive x-ray detector with 200 by 200 resolution elements, (3) on-line computer system for data acquisition and display, and (4) an ultra-high-speed interface between the detector electronics and computer memory. The current design of the

²⁵Abstract of paper published in *Philos. Mag.* 30(4): 819-37 (1974).

²⁶Institut für Festkörperforschung der Kernforschungsanlage, Jülich, West Germany.

²⁷J. Schelten and R. W. Hendricks, "A New Small-Angle X-Ray Scattering Facility Utilizing a Rotating Anode, Pin-Hole Collimation and a Position-Sensitive Proportional Counter," *Journal of Applied Crystallography*, in press.

interface is capable of converting the position of the incident x ray from two analog-to-digital converters into an absolute memory address in the computer, incrementing that location and testing it for overflow at over 10^5 events/sec. Extension to over 5×10^5 events/sec is possible with minimal modifications. We anticipate that the presently available 6-kW rotating anode x-ray source will be replaced with a 60-kW source in the next year, thus giving sufficient power to detect about 0.1% swelling in specimens 1 mm diam by 0.001 mm thick.

1.2.11 Quantitative X-Ray Fluorescence Analysis Using Fundamental Parameters²⁸ - C. J. Sparks, Jr.

The use of a monochromatic source of x rays for excitation permits direct and relatively simple calculations to be made to quantify the measured fluorescent intensities on an absolute basis of weight per unit weight of sample. Only the mass absorption coefficients of the sample for the exciting radiation and the fluorescent radiation need to be determined. Besides the techniques for the direct measurement of these absorption coefficients, other solutions are considered, which require fewer sample manipulations and measurements. Experimental measurements are described that permit the determination of nonhomogeneous matrix interference effects. Results are given for several kinds of samples. These methods permit quantitative analysis without recourse to the time-consuming process of preparing standards.

1.2.12 Effects of Neutron Irradiation on the Long-Range Order and Superconducting Temperatures of Nb₃Sn - C. J. Sparks,²⁹ R. Bett,³⁰ and B. A. Bellamy³⁰

Studies of neutron irradiation on Nb₃Sn superconducting tapes have related the atomic order of the A15 compound to the critical superconducting transition temperature, T_c . As shown in Fig. 1.1(a), neutron fluences in excess of 10^{19} n/cm² will lower T_c below that useful for magnets. Annealing for about 4 hr at 750°C will recover the critical temperature, which is directly related to the amount of order in the A15 structure. Figure 1.1(b) shows the volume changes undergone in a cross section of the superconducting tape upon irradiation. The Nb₃Sn expands normal to the niobium substrate on irradiation, placing niobium in tension in the plane of the tape. Annealing at 450°C for a few hours will relax this elastic strain without changing the degree of order. As the anneal does not change the critical

²⁸Abstract of invited paper for 24th Annual Denver X-Ray Conference, Denver, Col., Aug. 6-9, 1975.

²⁹Work performed while on assignment to AERE, Harwell, England.

³⁰Members of the staff, AERE, Harwell.

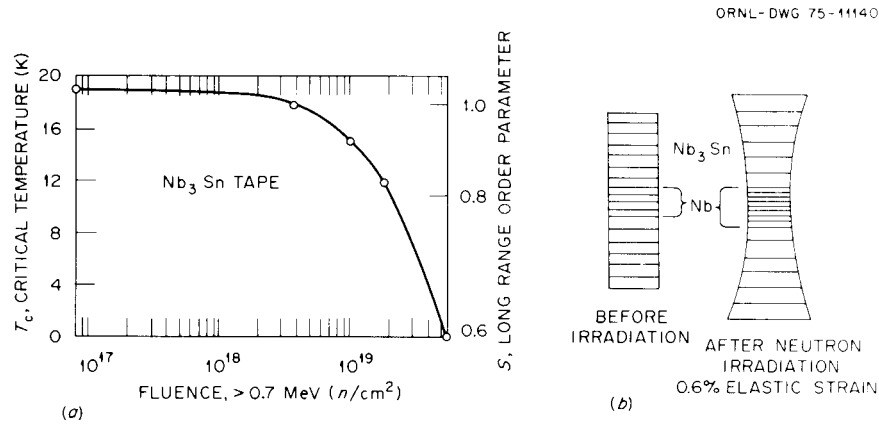


Fig. 1.1. Effect of Neutron Irradiation at 70°C on Nb_3Sn Superconducting Tape. (a) Decrease in critical temperature, T_c , and long-range-order parameter, S , as a function of neutron dose. (b) Elastic strains introduced by the differential expansion of Nb_3Sn and the niobium substrate.

temperature, we conclude that T_c in Nb_3Sn is unaffected by elastic strain to 0.6% and depends mostly on the amount of long-range order.

1.3 ALLOY STRUCTURE — R. O. Williams

Many technologically important alloys are solid solutions, and the atomic disorder induced by the alloying process influences the chemical and mechanical properties of the alloys. A better understanding of these structural effects is essential in order to predict the intrinsic stability of alloys and to evaluate radiation effects and the potential for long-term property changes in structural components of energy generating systems.

The specific goal of this research is to characterize the disorder in solid-solution alloys in terms of its influence on the thermodynamic properties of the alloys and to describe it through analyses of the diffuse x-ray scattering phenomena. Our work thus encompasses the application of solution thermodynamics to alloy systems and the analysis of x-ray diffraction phenomena exhibited by alloys.

1.3.1 Computer Simulation of Solid Solutions — R. O. Williams

We have developed and used a computer program that simulates the rearrangement of the atoms in a random binary mixture so as to make the resulting atomic distributions in the immediate neighborhoods of the atoms agree with experimental x-ray results. In order to get the desired statistical significance, it is essential that the model contain a large number of atoms, and in order to get agreement with the x-ray results,

it is necessary to extend the neighborhoods being examined to several hundred atoms. Such modifications result in substantial increase in computational time, so the original program has been rewritten to make it more efficient. It has been extended to provide various kinds of characterization of the finished model. In particular, the x-ray intensity calculated for the model is compared with the observed intensity.

1.3.2 The Nature of the Limitations of Second Law Determinations of Solution Thermodynamics³¹ - R. O. Williams

The unreliability of the entropy and heat of mixing of solutions deduced solely from free energy measurements results from systematic errors in the data and the lack of information on the temperature dependence of the heat of mixing. If one could predict the entropy in the high-temperature limit then one needs to solve only one of these problems. The temperature dependence of the heat of mixing cannot be satisfactorily deduced from the free energy and must be measured calorimetrically. The finite sensitivity of the free energy measurements, which has previously been blamed as the origin of this problem, is not necessarily an important factor.

1.3.3 The Importance of Multiple X-Ray Scattering in Measurements of Diffuse Intensity³² - R. O. Williams and C. J. Sparks

Calculations by others of double-diffuse and multiple Bragg scattering have been made for amorphous and polycrystalline materials, respectively. We have now treated the situation of diffusely scattered radiation undergoing Bragg scattering as well as the case of a Bragg-scattered beam being subjected to a diffuse scattering process before emergence from the sample. In both instances intensity may be added to or subtracted from the diffuse intensity of interest. We treat these two cases in terms of the geometrical positions in reciprocal space at which enhancement or reduction of the measured intensity can occur. One example of these multiple scattering effects is provided by the diffuse intensity measured from a fcc single crystal of Cu-16 at. % Al. The positions in reciprocal space that coincide with Bragg scattering of the incident or detected radiation are plotted and shown to occur at positions where differences are found between observed and calculated intensities. An example of secondary Bragg scattering is given by the thermal diffuse scattering measurements made on hot-pressed pyrolytic graphite.

³¹Abstract of paper published in *Mater. Sci. Eng.* 19: 37-42 (1975).

³²Abstract of paper prepared for publication.

1.3.4 Flip-Flop Decomposition Within Miscibility Gaps³³ — R. O. Williams

A local perturbation that is sufficiently stable to grow can lead to a flip-flop type of decomposition within a miscibility gap without subsequent nucleation. This process must occur if the surrounding matrix is essentially unchanged. This model is invoked to explain the higher regular plate structures that are observed, structures that appear to have a degree of regularity greater than that predicted by Cahn's theory of spinodal decomposition. The origin of the plate structure is associated with anisotropic energy factors, and in the absence of such factors the flip-flop mode of decomposition would lead to a Swiss-cheese structure, which would be extremely difficult to distinguish from that predicted by Cahn's theory. During coarsening the platelike structure can be retained through the successive elimination of individual plates without changing the essential nature of the structure.

1.4 FUNDAMENTAL CERAMICS — J. Brynestad

This group conducts research on refractory materials and on reactions between ceramics, metals, and corrosive environments, in support of various energy programs.

1.4.1 Refractory Europium Compounds — J. Brynestad and S. L. Bennett

A program has been initiated to investigate the properties of europium compounds of potential importance to the development of alternate advanced fast-neutron absorbers for the LMFBR. Efforts have begun in the areas: (1) preparation of single crystals of Eu_2O_3 for crystallographic, thermal expansion, and thermal conductivity studies, (2) preparation and investigation of the properties of EuO , (3) investigation of the existence of europium-rich phosphides, and (4) investigation of ternary compounds in the systems Eu-B-C and Eu-B-N .

1.4.2 Surface Properties of Europium Oxide: Initial Studies — H. F. Holmes³⁴

The adsorption of nitrogen (at 77°K), argon (at 77°K), water (at 20°C), and carbon dioxide (at 20°C) on cubic europium oxide was measured with a vacuum microbalance. This sample had a specific surface area of 5.79 m²/g and was nonporous, as evidenced by the reversibility of the nitrogen and argon isotherms. Water and carbon dioxide sorption was complicated by an

³³Abstracted from paper submitted to *Journal of Materials Science*.

³⁴On loan from Chemistry Division.

initially fast chemisorption accompanied by reversible physical adsorption and a very slow irreversible adsorption. The amount of irreversibly adsorbed water was larger than could be accounted for with a simple one-layer chemisorption model (this was true also for carbon dioxide). At the present time, it is not clear whether the slow irreversible adsorption of water (or carbon dioxide) is a bulk process or the formation of a complex surface compound. Projected studies include similar experiments with the monoclinic form of europium oxide. This research relates to the storage stability of fast-neutron control rods fabricated from europium oxide.

1.4.3 Unidirectional Solidification of Eu_2O_3 -Mo Composites -
A. T. Chapman,³⁵ J. Brynestad, and M. B. Watson³⁵

Molybdenum-fiber-reinforced and doped Eu_2O_3 was grown by directional solidification. This may be of potential significance for the development of crack-resistant europia fast-neutron absorbers.

1.4.4 Thermodynamic and Chemical Properties of Transition Metal Tellurides - J. Brynestad, S. L. Bennett, and R. E. Clausing

Thermodynamic properties of selected transition metal tellurides are being studied with a TGA/DTA unit. The distribution of tellurium between the bulk phase and the grain boundaries in nickel is being studied by means of Auger spectroscopy and chemical analysis. The results demonstrate that tellurium has a very strong preference for the grain boundaries in pure nickel. Studies are under way to investigate the nature of intergranular attack by tellurium on nickel-base alloys.

1.4.5 Crystallization of Eu_2O_3 and of Eu_2O_3 -Containing Compounds From Molten-Salt Solvents in the Range 900-1400°C - S. L. Bennett, C. B. Finch, and H. L. Yakel

Mass transport of Eu_2O_3 was achieved over a 30°C temperature gradient from surplus Eu_2O_3 in NaF solvent at 1150 to 1180°C. The recrystallization product was Eu_2O_3 plates and needles less than 1 mm in length, and the Eu_2O_3 solubility in NaF was estimated to be less than 5 mole %. Use of NaF- EuF_3 solvent resulted in deposition of EuOF , and EuCl_3 gave EuOCl at 900°C. All experiments were conducted in sealed platinum vessels and an atmosphere of dried argon. Also studied were the nonhalide solvents Eu_2O_3 - CuO - Cu_2O and Eu_2O_3 - Na_2O - B_2O_3 , which resulted in crystallization of EuCuO_2 and EuBO_3 at 1400 and 1200°C, respectively.

³⁵Consultant from the School of Ceramic Engineering, Georgia Institute of Technology.

1.5 CRYSTAL PHYSICS — G. W. Clark

The growth of crystals of refractory materials is our central theme. Frequently very specific crystals (composition, phase, purity, perfection, size, etc.) are required to characterize physical properties uniquely or are required in technical devices for their optimum operation. Such suitable crystals are often difficult to obtain; hence, we are conducting a continuing program to devise and improve methods of crystal growth, to develop increased understanding of crystal growth processes and kinetics, and to provide crystals needed in research. Crystals are grown by several methods: by internal zone growth, by temperature-gradient zone melting, from molten-salt solvents, from supercritical aqueous systems, by edge-defined film-fed growth, and by the Verneuil method. During this report period, our crystals were shared for investigating electron spin resonance, optical and elastic properties, deformation, diffusion, field emission, and electronic oscillator quality. We are investigating selected physical properties, both those related to the crystal growth process and those important for characterizing new compounds and eutectic structures. Of specific consideration is the use of metal oxide-metal eutectic composites as MHD electrode material and turbine components.

1.5.1 Directional Solidification by Internal Zone Melting of Cr₂O₃-Mo Composites — J. D. Holder and G. W. Clark

Studies of metal oxide-metal eutectics with Cr₂O₃ or (Cr,Al)₂O₃ matrices are under way. The most recent information places the Cr₂O₃ eutectic equilibrium composition at approximately 11 mole % Mo. To date we have successfully used internal zone melting to grow off-eutectic composites of Cr₂O₃-28, -35, and -40 mole % Mo. While we are not certain as to whether we have achieved steady-state conditions during directional solidification, we have grown a dendrite-free, rod-type eutectic at growth rates up to 5 cm/hr, even for the composition Cr₂O₃-40 mole % Mo. We also have confirmed that the criterion $\lambda^2 R = \text{constant}$ is met in areas where at least near-steady-state conditions exist. We have shown that rigorous thermomechanical calculations, where metastable oxide species are considered, can be used to predict the optimum oxygen pressure for successful internal zone melting and directional solidification in the system Cr₂O₃-Mo. Improper control of the furnace atmosphere can result in a failure to melt or in large sample losses by oxidation of molybdenum or reduction of Cr₂O₃ at oxygen pressures where simple free energy calculations would predict stability.

1.5.2 Experimentally Scaling Up Internal Zone Growth — A. T. Chapman³⁵
and G. W. Clark

A number of applications that require large volumes of the eutectic materials (i.e., MHD electrodes, electronic components, turbine components, etc.) has developed. Consequently, the scale-up of our technique of directional solidification by internally zone melting to larger samples is under investigation. Since we have the most experience with UO₂, it was selected as the material for the first effort. Previously the diameter of the molten zone has been 9 to 12 mm. In seeking to produce a molten zone of twice this diameter (20–25 mm), we constructed an enlarged system to accommodate a green pressed UO₂ bar of 31 mm diameter. During these tests, no significant differences in the melting and solidification procedures were encountered. A power increase of only 60% was required for samples having melt-zone diameter of 16 mm as opposed to 10 mm (i.e. a ratio of melt areas of 2.5). This trend is in support of the conclusions of mathematical modeling. Similar tests are now in progress using the eutectic UO₂-W.

1.5.3 Mathematical Modeling of Internal Zone Growth — R. A. Hartzell,³⁶
R. F. Sekerka,³⁷ J. D. Holder, and G. W. Clark

A collaboration between Carnegie-Mellon University and ORNL has been initiated to develop a model of the internal zone growth technique. The purpose is to utilize the predictive capacities of this model to improve present internal zone growth systems and to extend the use of this general method. The Carnegie-Mellon staff is modeling the relationships involving eddy-current heating in an inductively heated material whose electrical conductivity increases rapidly with temperature. The influence of processing parameters and material properties on the liquid zone shape will be illustrated with computer-generated profiles of the isotherms and electromagnetic fields. An experimental program is started at ORNL to relate the computer-generated profiles with the internal zone growth of silicon.

³⁶Graduate student, Department of Metallurgy and Materials Science, Carnegie-Mellon University. Work supported by ERDA subcontract by the Office of Materials Science, Division of Physical Research.

³⁷Faculty, Department of Metallurgy and Materials Science, Carnegie-Mellon University. Work supported by ERDA subcontract.

1.5.4 The Directional Solidification of Pb-Sn-Cd Alloys — J. D. Holder³⁸
and B. F. Oliver³⁹

The growing interest in composite structures for new material applications makes it necessary to determine just how generally we can apply existing solidification theory to controlled three-phase ternary solidification. The Pb-Sn-Cd ternary eutectic system was used as a model to map completely the phase morphology as a function of ratio of growth to temperature gradient (G/R) and composition. By carefully controlling the freezing rate and the thermal gradient in the liquid ahead of the solid-liquid interface (in the range 40–50°C/mm) the following areas of interest were investigated: (1) the effect of growth velocity and composition on coupled structures, (2) ternary impurities and their effect on the minimum G/R for coupled growth in a binary system, (3) the effect of growth velocity and composition on the nonplanar interface structures, and (4) the adaptability of present theories (the constitutional supercooling criterion and Cline's binary analysis) in predicting the region of coupled growth in a three-component eutectic system growing at steady-state. Much of the one- and two-phase directional solidification theory and terminology could be directly extended to a ternary eutectic system. This suggests a further extension to n -phase, m -component system ($m \geq n$) with at least a qualitative understanding of the solidification process.

1.5.5 Unidirectional Solidification of a MnO-Mn₂SiO₄ Eutectic by the Edge-Defined, Film-Fed Method — G. W. Clark, C. B. Finch,
J. D. Holder, and H. L. Yakel

To provide a better understanding of heat flow, thin film, capillary, and die geometry effects in the EFG⁴⁰ technique, we have grown cylindrical samples of off-eutectic MnO-Mn₂SiO₄. Samples have been prepared with different die surface shapes (i.e., planar, concave, and convex), over a broad range of growth velocities, and over a range of compositions. Metallography has revealed MnO fibers 2 to 3 μm in diameter, existing in colonies in a single-crystal Mn₂SiO₄ matrix. The preferred crystallographic

³⁸J. D. Holder is a member of the staff of Oak Ridge National Laboratory. This contribution is based upon his Master of Science Thesis in Metallurgical Engineering.

³⁹Professor in Charge of Metallurgical Engineering at the University of Tennessee, consultant to the Crystal Physics Group.

⁴⁰H. E. LaBelle, Jr. and A. I. Mlavsky, "Growth of Controlled Profile Crystals from the Melt: Part I — Sapphire Filaments," *Mater. Res. Bull.* 6: 571–80 (1971); H. E. LaBelle, Jr., "Growth of Controlled Profile Crystals from the Melt: Part II — Edge-Defined Film-Fed Growth (EFG)," *Mater. Res. Bull.* 6: 581–89 (1971).

alignment of the MnO fibers (cubic) relative to the matrix (orthorhombic) is being determined by x-ray diffraction. Rod discontinuities on a plane parallel to the solid-liquid interface (banding) have been observed at growth rates of 10 mm/hr or slower and are believed to be caused by a periodic fluctuation in interface location and/or by non-steady-state diffusion fields in the liquid film. This phenomenon, which is currently being investigated, may be very important.

1.5.6 Effect of Temperature on the Self-Luminescence of SrCl₂ Doped with ²⁴⁴Cm or ²⁵³Es: Observation of Host Defect Emission⁴¹ - C. B. Finch and J. P. Young⁴²

The self-luminescence of SrCl₂ crystals doped with ²⁴⁴Cm or ²⁵³Es was studied at 77 to 700 K in the wavelength range 300 to 700 nm. Two types of emission spectra were observed for either dopant, depending on sample temperature. The 77 K to room-temperature spectrum corresponds to a predominant blue, and the 500 to 700 K spectrum to a predominant yellow-orange emission. The luminescence intensity at 500 to 700 K remains relatively constant with time, suggesting the possible application of this material as a radioisotopic light source in this temperature region.

1.5.7 Growth of Single-Crystal Mn₂SiO₄ (Tephroite) by Czochralski and Edge-Defined, Film-Fed Techniques⁴³ - C. B. Finch, G. W. Clark, and O. C. Kopp⁴⁴

Optically transparent single crystals of Mn₂SiO₄ (tephroite) were grown by the Czochralski method in sizes up to 10 mm diam by 30 mm long. Growth was achieved from melts contained in platinum crucibles at 1313 ± 5°C under an atmosphere of moist Ar-4% H₂ [P_{O₂} ≈ 10⁻¹⁰ atm (10 μPa)]. Samples were also prepared by the edge-defined film-fed growth method (EFG), which confirmed the importance of maintaining a 2MnO:SiO₂ melt stoichiometry to obtain the optimum crystal quality. The resulting crystals were characterized by x-ray diffraction and optical methods. Mn₂SiO₄ is transparent to infrared radiation to 5 μm, and appears rose-colored to transmission in the visible.

⁴¹Accepted for publication in *Journal of Inorganic and Nuclear Chemistry*.

⁴²Analytical Chemistry Division.

⁴³Accepted for publication in *Journal of Crystal Growth*.

⁴⁴Consultant from the Department of Geological Sciences, University of Tennessee, Knoxville.

1.5.8 EPR Investigations of $^{253}\text{Es}^{2+}$ in Single Crystals of BaF_2 and SrCl_2 ⁴⁵ — M. M. Abraham,⁴⁶ C. B. Finch, L. A. Boatner,⁴⁷ and R. W. Reynolds⁴⁷

The EPR spectra of divalent ^{253}Es ($5f^{11}$ configuration) have been observed in the fluorite-structure hosts of BaF_2 and SrCl_2 . Spectra obtained for both hosts at about 24 GHz and 4.2 K exhibit a well-resolved, eight-line hyperfine pattern ($I = 7/2$). The magnetic field positions of the observed transitions were independent of applied field orientation, but line width anisotropies were present. The measured electronic g -values were significantly different for the two hosts, indicating that the ground state is a Γ_6 doublet for BaF_2 and a Γ_7 doublet for SrCl_2 . This behavior is similar to that exhibited by Ho^{2+} ($4f^{11}$ configuration) in these same two hosts. In view of the known importance of intermediate coupling effects for the spectra of actinide ions, the observation of a ground state crossover for Es^{2+} , which is analogous to that found for Ho^{2+} , is remarkable.

1.5.9 Measurement of Q for RbOH-Grown Quartz⁴⁸ — O. C. Kopp⁴⁴ and P. A. Staats⁴⁹

Studies of quartz crystals have shown a linear relationship between extinction coefficient α at 3500 cm^{-1} and acoustic loss Q . Some time ago we presented data relating $\alpha(3500\text{ cm}^{-1})$ to growth parameters (temperature in the growth region and growth rate) for RbOH-grown quartz, but because of the small size of the crystals we were not able to provide any Q measurements. Recently, we obtained a crystal of sufficient size to permit the direct measurement of both Q and $\alpha(3500\text{ cm}^{-1})$. The crystal was grown under the following conditions: solvent, 0.5 N RbOH; growth temperature, $458 \pm 5^\circ\text{C}$; base temperature $488 \pm 5^\circ\text{C}$; pressure, 1.2 ± 0.1 kbar (0.12 GPa); growth rate, 0.36 mm/day; seed, AT-cut. The temperatures were measured with externally strapped thermocouples. The values of $\alpha(3500\text{ cm}^{-1})$ and Q obtained for this crystal were 0.15 and 1.5×10^6 , respectively.

This single data point does not fall on curves relating $\alpha(3500\text{ cm}^{-1})$ and Q for either NaOH or Na_2CO_3 [an $\alpha(3500\text{ cm}^{-1})$ of 0.15 for these latter solvents corresponds to a Q of only about 0.8 to 0.9×10^6]. The offset position of the data point for RbOH-grown quartz may be related to

⁴⁵Presented at International Conference on the Electronic Structure of the Actinides, Argonne National Laboratory, October 1974.

⁴⁶Solid State Division.

⁴⁷Advanced Technology Center, P.O. Box 6144, Dallas, Texas 75222.

⁴⁸Abstracted from *J. Phys. Chem. Solids* 36: 356 (1975).

⁴⁹Physics Division.

differences in the absorption spectrum for Rb^+ -grown quartz as compared with Na^+ -grown quartz. Alternatively, the data may reflect a higher degree of intrinsic perfection of Rb^+ -grown quartz. If so, then it may be possible to grow more perfect quartz using rubidium-base solvents than is now being grown using sodium-base solvents.

2. DEFORMATION AND MECHANICAL PROPERTIES

R. A. Vandermeer

The cornerstone of Materials Science as a discipline is founded on the basis that important relationships exist between the microstructure of a material and its properties. This group seeks to establish these relationships, with particular emphasis on mechanical behavior, in materials of relevance to nuclear and other energy-related fields. We also search to discover, characterize, and understand new patterns of behavior, such as the reverse-shape-memory effect. The unique materials we investigate include uranium alloys, pyrocarbon coatings, and high-conductivity aluminum alloys.

2.1 AGING-INDUCED SHAPE INSTABILITY IN AN ELASTICALLY BENT U-7.5 wt % Nb-2.5 wt % Zr ALLOY; A REVERSE SHAPE MEMORY EFFECT — R. A. Vandermeer

The U-7.5 wt % Nb-2.5 wt % Zr alloy when quenched from 1073 K (800°C) exists at room temperature as a metastable phase, which is a slight tetragonal distortion of the elevated-temperature bcc phase. Flat, as-quenched specimens have been elastically deformed in four-point bending to maximum outer fiber stresses below the stress required for plastic deformation but into a range of stress where pseudoelastic behavior has been observed. Aging of these elastically bent specimens at 423 K (150°C) while constrained by the bending fixture resulted in a permanent deflection and shape change. Further isothermal aging after removal from the bending apparatus caused increasing deflection and continued shape instability in spite of the absence of the applied load. X-ray examination of samples cut from a bent and aged specimen revealed important preferred orientation and lattice parameter differences between the tension and compression regions and the high- and low-stress parts of the specimen. These observations were compared with previous findings on quenched samples of this alloy that had been either deformed separately or aged separately. A rationalization of the shape instability was put forth and may be summarized as follows:

1. Deformation during elastic bending was accomplished primarily by a twin nucleation and growth process.
2. Because of the nonuniformity of stress state in bending and the strong stress-directional dependence of twinning on crystal orientation, a unique kind of preferred orientation (texture) developed during elastic bending; the tetragonal a axis tended to align parallel to the tension stress, while the c axis lined up with the compressive stress.
3. Aging under constraint allowed solute-atom clustering or segregation to pin the twin interfaces, causing a permanent deformation when the load was removed.
4. Because the a lattice parameter expanded and the c parameter contracted on further unconstrained aging and because of the preferred alignment of these directions on the tension and compression sides of

the specimens, respectively, a continued deformation took place even though no load was imposed.

5. Much of the bending deformation could be removed without the aid of an applied stress by reheating to 673 K (400°C). The solute clusters dissolved, twin boundaries became unpinned, and the twins — still being elastic — receded and the material straightened.

Further work is under way to understand quantitatively and to predict this and other shape memory effects in uranium alloys.

2.2 TRANSMISSION ELECTRON MICROSCOPY OF PROPENE-DERIVED PYROLYTIC CARBON¹ — C. S. Yust and H. P. Krautwasser²

The microstructures of pyrocarbon coatings deposited under a wide range of conditions have been investigated by means of transmission electron microscopy. A complete understanding of the specific structures formed under known deposition conditions and the relationship of these structures to deformation and irradiation damage effects are necessary for optimization of the coating. The analysis of specimens deposited from Ar-20% propene (C₃H₆) at temperatures ranging from 1250 to 2000°C shows that structures formed under these conditions can be described in terms of three components. The low-temperature component (< 1400°C) consists of spherelike growth features approximately 0.5 to 1.0 μm in diameter of high density and fine crystallite size. At 1400°C, the microstructure contains spherical features composed entirely of fine, tangled fibers and is consequently very porous. As the deposition temperature increases, the coating becomes more dense as increasing amounts of a layer-structure pyrocarbon form at the outer edges of the porous growth features. The appearance of the structures as a function of temperature is in agreement with density measurements of the coatings and with the microporosity distribution in the coating as determined by small-angle x-ray scattering.

2.3 PRECIPITATION HARDENING IN ALUMINUM-GOLD ALLOYS — J. C. Ogle and R. A. Vandermeer

In the proposed underground superconducting power transmission lines, ultra-high-purity aluminum is a candidate material to carry fault currents and to provide a path for the rated current should the superconductor temporarily go normal. If the aluminum could also mechanically support the superconductor assembly certain design simplifications and weight savings might be realized. High-purity aluminum, though electrically suitable, is too weak. The purpose of this research has been to discover methods for producing a strengthened aluminum retaining reasonably high conductivity.

¹Abstract of a paper published in *Carbon* 13: 125-33 (1975).

²On assignment from Institut für Reaktorwerkstoffe, KFA, Jülich, Germany.

We are exploring the possibility of manipulating the dispersant in a dilute, precipitation-hardenable alloy whose solid solubility is extremely limited. Carefully characterized alloys of zone-refined aluminum (RRR = 13,000)³ containing 0.07, 0.12, and 0.26 wt % gold were melted, cast, homogenized, and fabricated into wires 2.6 mm in diameter. Aging treatments were carried out in salt baths at 371, 460, and 573 K (98, 187, and 300°C) on specimens cut from these wires after they were solution heat-treated for 57,000 sec at 913 K (640°C) and quenched into an ice-water brine solution at near 273 K (0°C). Aging times varied between 360 and 3.6×10^6 sec. After aging, RRR was measured, and representative data are summarized in Table 2.1. For comparison, data from pure aluminum are also listed. Substantial increases in RRR can obviously be achieved by aging. Transmission electron microscopic examination of the aged specimens is currently under way, as is monitoring the microhardness. We will establish relationships between microstructure (i.e., precipitate type, size, density, etc.), and RRR. We intend to investigate the mechanical properties of this alloy by tensile testing with the objective being to "map out" the relations between yield strength and RRR for various dispersion states.

³RRR = residual resistivity ratio ($\rho_{298 \text{ K}}/\rho_{4.2 \text{ K}}$).

Table 2.1. Residual Resistivity Ratio

Gold Content (wt %)	RRR Under Various Conditions			
	As Fabricated	SHTQ ^a	Aging Treatments	
			36,000 sec 460 K	3.6×10^6 sec 573 K
0.000	3953	3808	13,512	13,570
0.07	114	138	246	885
0.12	98	115	256	2,674
0.26	75	55	112	1,186

^aSolution heat-treated and quenched.

2.4 THE MICROSTRUCTURE OF COAL — L. A. Harris and C. S. Yust

The ultrafine pore systems in coal are under study by transmission electron microscopy. Improved knowledge of the fine pore structure of coal may contribute to the development of improved coal liquefaction and gasification processes. A thin slice of a low sulfur, high-volatile, bituminous coal was prepared for electron microscopy by argon-ion bombardment. The coal was found to contain several pore forms, one of which is shown in Fig. 2.1. In this instance, an aligned group of conical

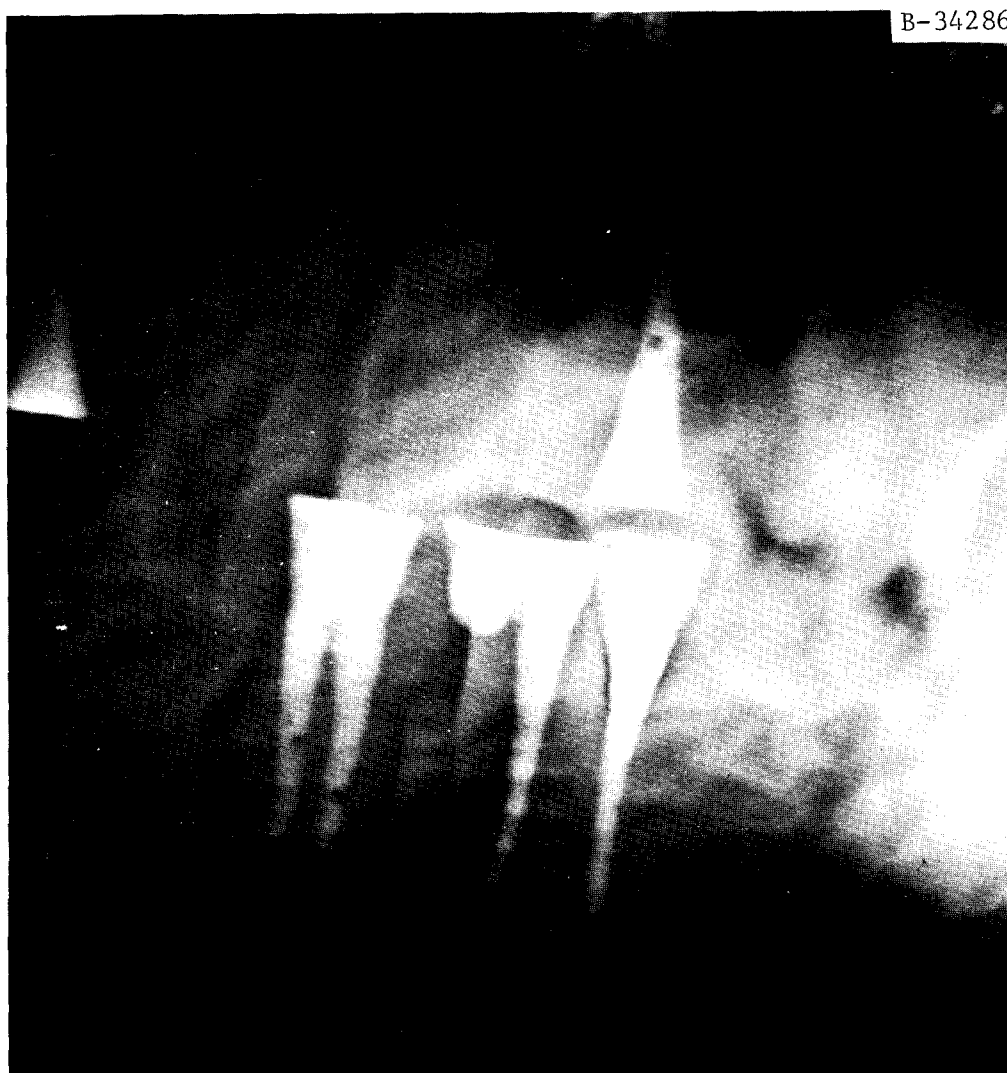


Fig. 2.1. Conical Voids Formed in a Coal Constituent. The small spherical particles (about 250 Å in diameter) near the heads of the voids are frequently observed in pores in coal.

voids apparently originates on the central plane of a particular coal constituent. The small spheres observed in many of the voids are also seen in nonconical voids, and are possibly responsible for the void formation by means of a catalytic reaction.

3. PHYSICAL PROPERTIES AND TRANSPORT PHENOMENA

3.1 PHYSICAL PROPERTIES RESEARCH — D. L. McElroy¹

The general goals of this effort are the generation of accurate thermal conductivity, electrical resistivity, specific heat, coefficient of thermal expansion, and Seebeck coefficient data for a variety of materials of immediate interest, materials of possible future interest, and materials that will lead to improved knowledge of the relation between the above properties. Parameters determined from the above properties can be used in what is sometimes a heuristic approach to provide information for systems where experimental data is nonexistent.

3.1.1 Lattice Thermal Conductivities in Electrically Insulating Crystals — J. P. Moore, R. K. Williams, R. S. Graves, T. G. Godfrey, F. Weaver, and D. L. McElroy

If experimental data are to assist in the resolution of lattice conduction problems in insulators, the thermal conductivity, λ , must be accurately determined over a wide temperature range scaled in terms of the Debye temperature, θ_D . One way this can be accomplished is to study materials with low θ_D since techniques that have a limited temperature range can yield data at high values of T/θ_D without measurements at absolute high temperatures, where experimental difficulties are increased. This factor alone makes some of the alkali halides of interest.

We measured² λ of RbBr, RbI, and RbCl over the temperature range from 80 to 400 K with minimum uncertainties of $\pm 2.5\%$ at 80 K. The data were corrected for photon conduction, but the correction uncertainties caused the overall measurement uncertainties to increase with increasing T . These results disagree with results from others by as much as a factor of 4. The data were compared with an approximate equation for three-phonon umklapp scattering involving only acoustic-mode phonons. The deviation of experimental thermal resistance ($1/\lambda$) values from calculated values increased smoothly with increasing mass ratio, as shown in Fig. 3.1. This trend continues for our recent data on CsCl. Results³ on KCl are also near this smooth curve. This smooth increase with mass

¹On assignment to AERE, Harwell.

²J. P. Moore, R. K. Williams, and R. S. Graves, "Lattice Thermal Conductivities of RbBr, RbI, and RbCl from 80 to 400 K," *Phys. Rev. Ser. B.* 11(8): 3107-15 (1975).

³P. J. Anthony and J. C. Wurst, "Thermal Conductivity of KCl Alloys," *J. Am. Ceram. Soc.* 57(11): 504 (1974).

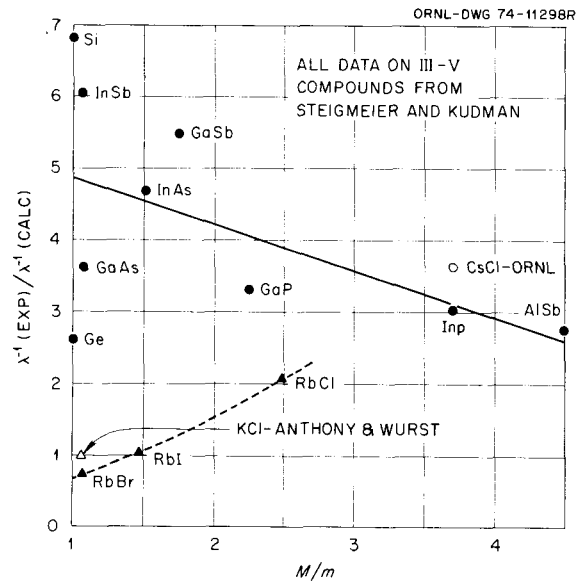


Fig. 3.1 The Ratio of Experimental to Calculated $1/\lambda$ for the Ionic Compounds RbBr, RbI, RbCl, CsCl, and KCl, plotted against mass ratio. Results from Steigmeier and Kudman [*Phys. Rev. Ser. B* 141: 767-74 (1966)] on the III-V compounds and group IV elements are also shown.

ratio is not true of the III-V compounds⁴ and group IV elements as also shown in Fig. 3.1.

The presence of significant four-phonon umklapp scattering processes in the rubidium halides cannot be excluded because of the high-temperature behavior of $1/\lambda$. Distinct slope changes in $1/\lambda$ near the Debye temperatures, which were observed in silicon and ThO_2 , were not detected in any of the alkali halide compounds, although the effect could have been masked by the experimental uncertainties. According to Anthony and Wurst,³ the addition of RbCl or KBr to pure KCl lowers λ . For the KCl alloys we have calculated⁵ values that are in good agreement with their experimental values.

We have completed the measurements of the thermal conductivity of hot-pressed monoclinic Eu_2O_3 over the range 87 to 1200 K, employing three different techniques. The three samples measured had different densities, and all results were corrected to a common density for comparison. Over the temperature range of overlap for the three techniques, all corrected results agreed to within $\pm 1\%$. The thermal conductivity of Eu_2O_3 decreases with increasing temperature, but the rate is less than $1/T$. Detailed analysis of these results is in progress.

⁴E. F. Steigmeier and I. Kudman, "Acoustical-Optical Phonon Scattering in Ge, Si and III-V Compounds," *Phys. Rev. Ser. B* 141: 767-74 (1966).

⁵J. P. Moore and T. G. Godfrey, "Comment on 'Thermal Conductivity of KCl Alloys'," *J. Am. Ceram. Soc.* 58(7-8): 344 (July-August 1975).

3.1.2 Physical Properties of Metals

3.1.2.1 Chromium⁶ — J. P. Moore, R. K. Williams, and R. S. Graves

The thermal conductivity, λ , electrical resistivity, ρ , and Seebeck Coefficient, S , of a high-purity chromium specimen ($\rho_{273}/\rho_{4.2} = 380$) were measured⁵ from 280 to 1000 K. The ρ and S of two other chromium specimens ($\rho_{273}/\rho_{4.2} = 380$ and 58) were determined from 300 to 1300 K. The ρ and S results from the three specimens were in excellent agreement, and the measurements of all three properties agreed, within experimental uncertainty, with previous low-temperature results on the same specimen over the temperature range of overlap. Near the Néel temperature (300–320 K), the present λ results were within 0.7% of the previous data, and indicated that $\lambda\rho/T$ should be smooth to within 1%. At high temperature the present λ data were about 8% above those of Powell and Tye,⁷ but this appears to be caused by purity difference since the ratios of $\lambda\rho/T$ agreed to within 2% up to 1000 K.

3.1.2.2 Tungsten⁸ — R. K. Williams

The electrical resistivity, ρ , of a zone-refined tungsten sample (residual resistivity ratio 7×10^4) was determined between 1100 and 2500 K. The error analysis indicates that the data are accurate to about 1%, and comparison of the results with other ρ data indicates that the error analysis may be pessimistic. The effects of thermionic charge transport on the ρ data and the performance of uninsulated W-3% Re vs W-25% Re thermocouples were also investigated. Comparison of the data with transport theory indicates that most of the nonlinear ρ behavior observed at high temperatures is due to thermal expansion effects.

3.1.2.3 Molybdenum — R. K. Williams, J. P. Moore, and R. S. Graves

Measurements on pure molybdenum⁹ and five molybdenum-base alloys (0.86% Ti, 1.07 and 2.06% Nb, 1.0 and 1.6% Zr) have now been obtained.

⁶Abstract of a paper "Thermal Conductivity, Electrical Resistivity, and Seebeck Coefficient of High-Purity Chromium," to be submitted for publication.

⁷R. W. Powell and R. P. Tye, "The Influence of Heat Treatment on the Electrical Resistivity and the Thermal Conductivity of Electrodeposited Chromium," *J. Inst. Met.* 85: 185 (1957).

⁸Abstracted from "A Study of the Electrical Resistivity of Zone-Refined Tungsten at High Temperatures," *J. Appl. Phys.* 46(2): 475–89 (February 1975).

⁹J. P. Moore, R. K. Williams, and R. S. Graves, *Rev. Sci. Inst.* 45: 87–95 (1974).

This work determined the relative contributions of electrons and phonons to the total thermal conductivity of molybdenum. The analysis of the results is incomplete, but the data indicate that the lattice conductivity has a maximum value near 125 K, and at this point phonons contribute 10 to 15% of the total thermal conductivity. The new results are also consistent with a previous¹⁰ suggestion that most of the difference between the thermal conductivities of tungsten and molybdenum is due to stronger electron scattering of the phonons in molybdenum.

3.1.2.4 Aluminum¹¹ — J. P. Moore

Measurements of λ , ρ , and S on three aluminum specimens of different purities were made using three separate techniques in a cooperative experiment with the National Research Council of Canada. All results were combined to determine λ , ρ , and S for pure aluminum from 20 to 400 K. The thermal conductivity has a broad plateau from 180 to 400 K and a possible minimum of 0.25%, which is within the experimental errors.

The ρ and λ of a sample of an 1100 aluminum alloy with a resistivity ratio of 17 were measured from 80 to 400 K. The measured values agreed to within $\pm 1\%$ with values calculated from parameters obtained from the pure-aluminum results.

3.1.2.5 Nickel-Base Alloys¹² — J. P. Moore, R. S. Graves, and R. A. Vandermeer

One of the most used thermocouples consists of Chromel vs Alumel, but this pair has large errors because of short-range order in the Chromel¹³ and oxidation of both materials at high temperatures.¹⁴ Such effects are

¹⁰R. K. Williams and W. Fulkerson, "Separation of the Electronic and Lattice Contributions to the Thermal Conductivities of Metals and Alloys," pp. 389-456 in *Thermal Conductivity, Proc. 8th Conf.*, ed. by C. Y. Ho and R. E. Taylor, Plenum Press, New York, 1969.

¹¹Synopsis of a paper "The Thermal and Electrical Conductivity of Aluminum," by J. G. Cook, J. P. Moore, T. Matsumura, and M. P. Vandermeer, to be published in proceedings of 14th International Thermal Conductivity Conference, Storrs, Conn., June 2-4, 1975.

¹²Abstracted from J. P. Moore, R. S. Graves, M. B. Herskovitz, K. R. Carr, and R. A. Vandermeer, *Nicrosil II and Nisil Thermocouple Alloys: Some Physical Properties and Behavior During Thermal Cycling to 1200 K*, ORNL-TM-4954 (August 1975).

¹³T. G. Kollie et al., *Temperature Measurement Errors with Type K (Chromel vs Alumel) Thermocouples Due to Short-Ranged Ordering in Chromel*, ORNL-TM-4862 (March 1975).

¹⁴N. A. Burley, "Nicrosil and Nisil: Highly Stable Nickel-Base Alloys for Thermocouples," *Temperature, Its Measurements and Control in Science and Industry*, Vol. 4, Instrument Society of America, Pittsburgh, Pa., 1972.

reduced in two nickel-base alloys that have been proposed for use as thermocouple elements, Nicrosil II (Ni-14.2% Cr-1.4% Si) and Nisil (Ni-4.4% Si-0.1% Mg-0.1% Fe). The thermal conductivities, electrical resistivities, and Seebeck coefficients of materials near to the above compositions were measured from 80 to 400 K, and the mean coefficients of thermal expansion were measured from 400 to 1100 K. The silicon in the Nisil lowers the Curie temperature of the base metal to about 290 K, where the Seebeck coefficient of the Nisil has a broad peak and the thermal conductivity has a small apparent discontinuity. The assumption that all electron scattering is elastic gives values for the lattice conduction component that are in good agreement with estimates from theory.

3.1.2.6 Specific Heat of ^{241}Am and $\text{PuC}_{0.8}$ ¹⁵ - D. L. McElroy

The specific heat, C_p , of actinide elements and compounds is being measured from 10 to 300 K with an adiabatic calorimeter.¹⁴ This method is applicable to encapsulated radioactive samples in which the heat generation due to radioactive decay may be large. An automatic potentiometer allows thermal emf-time data to be recorded in a form suitable for computer processing.

Samples of ^{241}Am and $\text{PuC}_{0.8}$ showed¹⁵ C_p anomalies below 100 K. If the ^{241}Am sample is held less than 1 hr below 77 K, a second-order transition occurs near 62.5 K with an estimated energy of 41 J/mol. Long-time holds below 10 K showed that the annealing of self-irradiation damage occurred in 3 stages below 200 K. A broad C_p anomaly, centered near 40 K, was noted for $\text{PuC}_{0.8}$ and may represent an antiferromagnetic transition.

3.1.3 Apparatus Development

3.1.3.1 Thermal Expansion Apparatus - T. G. Godfrey

The CODAS-operated coefficient of thermal expansion (CTE) apparatus was upgraded through replacement of the original electronic micrometer control with a solid-state unit. The original circuit, while of good design, used electromechanical relay logic and thermal time-delay relays. In operation, these devices proved to be unreliable.

¹⁵Work jointly sponsored by ERDA, ORNL, and AERE, Harwell. Abstracted from two papers: W. Muller, D. L. McElroy, R.O.A. Hall, and M. J. Mortimer, "The Specific Heat of Americium Metal from 15 to 300 K," and D. L. McElroy, R.O.A. Hall, and J. A. Lee, "The Specific Heat of PuC and Pu_2C_3 from 10 to 300 K," accepted for the 5th International Conference on Plutonium and Other Actinides 1975, Baden-Baden, Germany, Sept. 10-13, 1975.

The CTE apparatus was conceived as a steady-state, high-accuracy, and high-precision machine. Inherent in this approach is a very slow operation. Since more imprecise results might suffice for studies on some materials, the operation of the CTE apparatus under transient conditions was investigated. We found that the accuracy was decreased to 3% compared with the original 1%, by the transient mode, while the time required to obtain data decreased by a factor of 5. This mode is being used now for an investigation of the effects of volume fraction particle loading and irradiation on HTGR fuel sticks. For unirradiated control samples, the CTE increased linearly with volume fraction loading over the range 0 to 60% from 300 to 1000 K. After one cycle in the target region of the HFIR the two samples measured thus far had their CTE markedly reduced at 300 K, but to a lesser extent at higher temperature. We surmise that this decrease in CTE is caused by residual strain and micro-cracks in the matrix material.

3.1.3.2 CODAS Development — T. G. Godfrey

The Computer Operated Data Acquisition Systems, Phase III, has been installed in our laboratory. While based on a PDP8 8k-core computer similar to our CODAS Phase II system, Phase III is more advanced in its analog input circuitry and disk storage capacity. The first task for CODAS III is the operation of the Plane Probe apparatus.¹⁶ In addition, its unique capabilities are being extended by remote interfaces to experiments in both the Superconductivity and the Surface Phenomena Laboratories.

3.2 SURFACE PHENOMENA — J. V. Cathcart

The underlying goal of this research is to identify and characterize the various mechanisms of oxidation of alloys so that a rational basis may be provided for the design of oxidation-resistant alloys. As vehicles for this work we have chosen a series of uranium alloys, sets of refractory metal alloys based on tantalum and niobium, and several ceramic-metal composites. Phenomena being studied include the interrelationship of oxide morphology and the relative diffusion rates in the oxide and alloy, the effect of alloying elements on the defect concentration and diffusivity in the oxide, internal oxidation, grain boundary embrittlement, stress development, and oxygen solution effects.

¹⁶T. G. Godfrey and S. H. Jury, *The Plane Probe: A Transient Method for Rapidly Measuring Conductivity and Diffusivity of Salt Mine Core Samples*, ORNL-TM-4956, in preparation.

3.2.1 Oxidation of Uranium-Base Alloys

3.2.1.1 Current Investigations — G. J. Yurek, J. V. Cathcart, and G. F. Petersen

The oxidation rate of a metal in most circumstances is determined by the product of the defect concentration gradient and the defect diffusion coefficient in the oxide scale. Our previous attempts at measuring these quantities as functions of alloy composition and concentration for a series of uranium-base alloys using the "interrupted oxidation" technique has been hampered by difficulties associated with solving the appropriate diffusion equations. A computer code (see Sect. 3.2.3), based on a finite difference method, has now been written that should provide the desired solutions.

In a second approach to the problem of determining the defect diffusion coefficients and concentrations in oxide scales, we have derived equations that permit calculation of these quantities from the parabolic oxidation rate constants for diffusion-controlled oxidation reactions. Application of the equations requires the experimental measurement of the rate constants as a function of oxygen pressure. We will verify our equations using literature rate constant values for Cu_2O . Once validated, our theory will be applied to oxidation data for uranium and its alloys. This treatment should also be applicable to other types of oxidation reactions, such as sulfidation and nitridation.

3.2.1.2 The Development of Product Microstructures During the Diffusion-Controlled Oxidation of Uranium Alloys¹⁷ — G. J. Yurek

The development of product microstructures during the oxidation of alloys that form scales that exhibit predominant anion diffusion is considered. Wagner's analysis for scales that exhibit predominant cation diffusion is modified for the case of predominant anion diffusion. The variables expected to influence the product morphology are alloy composition, ambient oxygen pressure, and the relative mobilities for atoms in the alloys and anions in the scale. The theory is applied to the oxidation of uranium alloys that form two-phase (oxide + alloy) product layers in oxygen atmospheres.

¹⁷Abstract of paper to be presented at the Gordon Conference on Corrosion, New London, N.H., July 7-11, 1975.

3.2.1.3 Mechanisms of Stress Generation and Relaxation During the Oxidation of Uranium Alloys¹⁸ — J. V. Cathcart and G. F. Petersen

Very large stresses arise in the oxide scales during the oxidation of a variety of uranium alloys. The stress generation is related to the mode of diffusion in the oxide and to the oxide morphology. Several stress relaxation mechanisms are discussed. These include the creep of both oxide and substrate, cracking of the oxide, and a vacancy flow mechanism similar to Nabarro-Herring creep. Specific examples of these various phenomena are drawn from results obtained during oxidation of U-Nb, U-Mo, and U-Nb-Zr alloys.

3.2.2 Refractory Metal Alloys

3.2.2.1 Current Research — R. E. Pawel and J. J. Campbell

Tantalum- and niobium-base alloys exhibit significant oxygen solubility at high temperatures, and the dissolved oxygen greatly influences the oxidation and mechanical properties of the alloys. We have studied the diffusivity of oxygen in these materials. The effective diffusion coefficients of oxygen in pure tantalum, Ta-10 wt % W, and Ta-10 wt % W-2.5 wt % Hf were measured at 800 and 900°C as functions of grain size. The results indicate the importance of grain boundary diffusion of oxygen by the severe grain boundary embrittlement during the oxidation of tantalum alloys that we reported earlier.

To clarify further the role of hafnium in the oxidation of these alloys, we measured the diffusion coefficient of hafnium in tantalum. This work, carried out in cooperation with the Diffusion in Solids Group, indicated a value of about 10^{-18} cm²/sec for the lattice diffusion coefficient of hafnium at 900°C. Thus, it is evident that at the temperatures of our oxidation experiments hafnium is effectively pinned in the alloy lattice, although it could diffuse at an appreciable rate in grain boundary regions.

We have begun an investigation of the oxidation of two niobium alloys, Nb-1 wt % Zr and Nb-10 wt % Hf-1 wt % Ti. The former alloy exhibits essentially the same oxidation characteristics as pure niobium, although oxygen diffusion rates in the alloy were one-fourth as great. Initial results for the Nb-Hf-Ti alloy indicate a substantial reduction in oxidation rate relative to niobium in the early stages of oxidation, but the alloy is subject to the same grain boundary embrittlement and "ignition" phenomenon that we observed in tantalum-base alloys.

¹⁸Abstract of paper presented at the symposium on Growth Stresses and the Oxidation of Metals, Fall Meeting of the AIME, Detroit, Mich., Oct. 21-23, 1975. To be published in the proceedings in the symposium, J. V. Cathcart, ed.

3.2.2.2 Some Oxidation Characteristics of Ta-10% W and Ta-10 % W-2.5 % Hf Alloys¹⁸ - R. E. Pawel and J. J. Campbell

As part of a program on the oxidation behavior of refractory metal alloys, the early stages of oxidation of the alloys Ta-10 wt % W (Ta-10 W) and Ta-10 wt % W-2.5 wt % Hf-0.012 wt % C (T-222) were studied over the range 500 to 800°C in dry oxygen at atmospheric pressure. Both alloys exhibited a period of protective oxidation followed by an accelerating rate due, at the lower temperatures, to the initiation and lateral growth of high-rate regions consisting of porous nonprotective oxide. At the higher temperatures, the oxide film was more resistant to this form of breakdown and provided a comparatively longer period of protection.

The strain induced in specimens of these alloys during oxidation was measured by the flexure technique. The kinetics of flexure in the protective stage of oxidation in the above temperature range was determined and compared with the kinetics of oxidation. While high stresses undoubtedly existed in the oxide layers themselves, the major contributor to flexure under these conditions was judged to be oxygen solution effects in the alloys.

The experimental results are examined in terms of the kinetics of the reactions and the morphologies of the reaction products for the individual alloys and for unalloyed tantalum.

3.2.3 Computer Code Development - S. Malang¹⁹ and R. E. Pawel

A computer code has been written to simulate oxidation processes under a wide range of conditions. Using finite-difference techniques, the code provides solutions for the multiphase, moving-boundary diffusion problem in finite samples. Physical property data and kinetic and thermodynamic parameters serve as input to the code. The program may be used to generate phase thicknesses as a function of time, or, given experimental kinetic data, it can in principle extract diffusion coefficients and defect concentrations. It is presently being used in connection with our interrupted oxidation studies on uranium alloys (see Sect. 3.2.1.1), and we anticipate that it will be applicable to a number of future investigations.

3.2.4 Ceramic-Metal Composites - J. V. Cathcart and G. F. Petersen

In conjunction with the Crystal Physics and Fundamental Ceramics Groups we have started a program designed to characterize the chemical and mechanical properties of ceramic-metal composites at high temperatures in mixed-gas environments typical of the cooling gas stream of a gas-cooled reactor. Urania-tungsten composites were chosen as the initial material for this study because of their availability and because the reactions they undergo should be typical of although more severe than

¹⁹On assignment to ORNL from Karlsruhe Nuclear Research Center, Germany.

those for potentially more stable composites. Tests have been carried out in low-pressure oxygen, CO-CO₂ mixtures, and CH₄ at temperatures between 800 and 1100°C. Severe attack was observed in oxygen at pressures greater than about 0.05 torr (7 Pa), but only a slight leaching away of the ends of the tungsten fibers was found in CO-CO₂, CH₄, or low-pressure oxygen.

3.3 DIFFUSION IN SOLIDS — J. V. Cathcart

In any high-temperature system atom movement and material transport are possible, and the extent and nature of this transport may profoundly affect the physical and mechanical properties of the components of such systems. Thus, the phenomenon of diffusion is of fundamental concern in the design and operation of any high-temperature, energy-generating device based on the "heat engine" principle, and research of this group is designed to elucidate fundamental diffusion processes operative under these conditions.

Our work is divided between two general categories. The first involves studies of interdiffusion processes in alloys — that is, diffusion in the presence of chemical potential gradients. Special emphasis is being placed on achieving a better understanding of the vacancy wind phenomenon, an effect that arises during diffusion in alloys where the various components diffuse at different rates.

The second part of our program deals with interstitial diffusion in alloys and ceramics. The diffusing species are generally limited to the light atoms such as oxygen, nitrogen, carbon, and hydrogen and its heavier isotopes. This work is of potential significance in several ERDA programs, particularly in reactor projects such as the CTR, LMFBR, and MSBR, where the tritium containment problem is important.

3.3.1 Interdiffusion and Vacancy Wind Effects

3.3.1.1 Current Investigations — P. T. Carlson and L C Manley, Jr.

We are measuring interdiffusion, intrinsic diffusion, and vacancy wind parameters over the range 900 to 1600°C for a series of vanadium-titanium alloys. Analysis of the experimental data is still in progress, but initial results indicate vacancy wind effects to be appreciably greater than those predicted from theory.

Current theories for interdiffusion in multicomponent alloys (ternary or higher) predict that the nondiagonal terms in the general thermodynamic diffusion equation arise entirely from the vacancy wind effect and are no longer zero. Also, the diffusion rates of the various species in such an alloy appear to depend heavily on the magnitude of the nondiagonal terms relative to the diagonal coefficients. To test this effect, we have initiated a study of interdiffusion, intrinsic diffusion, and vacancy wind parameters in the V-Ti-Cr system at 1200°C. These results should be important in clarifying the vacancy wind phenomenon and in providing

a better basis for predicting vacancy movement and void formation in radiation-damaged material.

The following are abstracts of papers based on this phase of our work and published or submitted for publication during the past year.

3.3.1.2 MANTANØ — A Computer Code for the Analysis of Interdiffusion and Intrinsic Diffusion Information in Binary Systems²⁰ — P. T. Carlson

MANTANØ is a FORTRAN IV Computer Program written for the IBM 360/75 and 360/91 systems, it determines interdiffusion and intrinsic diffusion coefficients from the experimental concentration-penetration profiles of infinite and semi-infinite diffusion couples. The flexibility of the code enables the user to deduce experimental values of diffusion coefficients as well as to calculate expected values for any given system. The fundamental input array consists of the experimentally determined x-ray intensity-penetration data obtained from electron microprobe analysis of the diffused couples, which the program subsequently converts to concentration-penetration profiles by comparison with standards of known composition. An analytical expression describing the concentration of each species as a function of penetration is then determined by fitting low-order polynomial splines to the experimental data by the method of least squares. Subsequent calculations are performed on the regenerated profiles. Interdiffusion coefficients are determined at incremental penetration distances by the method of Boltzmann and Mantano with the use of Simpson's rule for integration. The analyses of Darken and Heumann are employed to calculate the experimental intrinsic diffusion coefficients at the composition of the Kirkendall reference plane. In addition, the program uses available thermodynamic and tracer diffusion coefficient information for the system of interest to predict theoretically values of diffusion parameters excluding and including consideration of the vacancy wind effect through the analyses of Darken and Manning, respectively. Experimental vacancy wind parameters, as well as atomic mobilities of the two species are determined by the method of Dayananda and are compared with the theoretical values. The output of the program provides the user with a rapid summary of the experimental and calculated information in tabular as well as graphical formats. Although MATANØ has been written with the assumption of constant molar volume across the diffusion zone, a correction can be made for molar volume changes due to composition differences by substitution of lattice spacing for diffusion distances.

3.3.1.3 Interdiffusion and Intrinsic Diffusion in Binary Vanadium-Titanium Solid Solutions at 1350°C²¹ — P. T. Carlson

Interdiffusion coefficients, intrinsic diffusion coefficients, and vacancy wind parameters have been determined in the vanadium-titanium

²⁰Abstracted from ORNL-5045 (June 1975).

²¹Abstracted from paper submitted for publication in *Metallurgical Transactions*.

system at 1350°C with the use of infinite, solid-solid diffusion couples. The experimentally determined coefficients were compared with the values predicted from the models of Darken, Manning, and Dayananda with the use of available tracer diffusion and thermodynamic information and were found to be larger than those calculated from these three models. Vacancy wind parameters, determined experimentally, reflect a greater influence of the vacancy wind phenomenon on the intrinsic diffusion flux of each species than that calculated on the basis of Manning's theory. In particular, the faster diffusing component is enhanced and the slower diffusing component is retarded to a greater degree than is theoretically predicted. Furthermore experimental and predicted values of intrinsic diffusivity ratio, D_V/D_{Tz} , were compared, and the results suggest an increased effect of vacancy flow on the intrinsic fluxes with respect to the magnitude of this phenomenon calculated from Manning's treatment. The vacancy wind effect is shown to be an important factor in the consideration of intrinsic diffusion fluxes and their relation to tracer diffusion and thermodynamic information in the vanadium-titanium system.

3.3.1.4 Atomic Mobilities and Vacancy Wind Effects for Diffusion in Ternary Silver-Zinc-Cadmium Solid Solutions²² — P. T. Carlson, M. A. Dayananda,²³ and R. E. Grace²³

Diffusion in the silver-zinc-cadmium system was investigated at 600°C with semi-infinite, vapor-solid couples in order to determine the atomic mobilities and contribution of the vacancy wind effect to the intrinsic diffusion fluxes of silver, zinc, and cadmium in the alpha phase region. Atomic mobilities and vacancy wind parameters were computed at selected compositions in the alpha phase along isoconcentration lines of 11 at. % Zn, 18 at. % Zn, 5 at. % Cd, and 9 at. % Cd. The existence of significant interactions between the diffusing species was indicated by the results of an earlier investigation;²⁴ consequently, the vacancy wind effect was taken into consideration in the calculation of the mobilities. The mobilities of zinc and cadmium, determined by the method of Dayananda, increased with increasing zinc and cadmium concentrations, and the mobility of zinc was greater than that of cadmium. The results of the investigation show that the vacancy wind effect significantly affects the total intrinsic flux of each of the three species for diffusion in ternary silver-zinc-cadmium alloys. This investigation reports the experimental observation of the vacancy wind effect in a ternary system.

²²Abstracted from *Metall. Trans.* 6A(6): 1245-52 (1975).

²³School of Materials Engineering, Purdue University, West Lafayette, Indiana 47907.

²⁴P. T. Carlson, M. A. Dayananda, and R. E. Grace, "Diffusion in Ternary Ag-Zn-Cd Solid Solutions," *Metall. Trans.* 8: 819-36 (1972).

3.3.2 Interstitial Diffusion — R. A. Perkins and R. A. Padgett

The diffusion rates of hydrogen through certain metal oxides are several orders of magnitude lower than the diffusion rates in the corresponding metals, a fact that may be of considerable significance in the solution of tritium containment problems. We initiated a study of the diffusion of hydrogen in oxides aimed at understanding the influence of stoichiometric defects in the oxide on the diffusion process. The system CoO-T is being investigated first because the defect structure of CoO is already well known.

We have also begun a study of interstitial diffusion in refractory metal alloys with the goal of defining the influence of alloying elements on diffusion rate. The system Nb-X-O, where X is Zr, Ti, or Mo, will be investigated over the range 700 to 1200°C.

3.4 SUPERCONDUCTING MATERIALS — C. C. Koch

We study the effects of metallurgical variables on the properties of superconducting materials. The superconducting property most structure sensitive appears to be current-carrying capacity in an applied magnetic field. It is affected by microstructural variables such as grain size, dislocation density and distribution, and morphology, composition, and volume fraction of second-phase particles. Meaningful correlation of structure and properties requires detailed knowledge of both. Consequently, some of our effort is devoted to obtaining basic metallurgical information on phase diagrams, transformation kinetics and products, and the microstructures that result from them in superconducting alloys systems. We correlate current-carrying capacity with the "model" microstructures.

We also study the influence of metallurgy on the basic superconducting property T_c , the superconducting-normal transition temperature. This property is controlled by alloying and, in compound superconductors, by degree of long-range chemical order. In conjunction with this part of our program we make low-temperature specific heat capacity measurements.

We have recently begun studies of power frequency ac losses in superconductors and of the relationship of mechanical strain under operating conditions to the superconducting properties of commercial Nb-Ti/Cu composites.

3.4.1 A Comparison of Methods for Measuring Flux Gradients in Type II Superconductors²⁵ — D. M. Kroeger, C. C. Koch, and J. P. Charlesworth²⁶

We compared four methods of measuring the critical current density, J_c , in hysteretic type II superconductors having a wide range of n and

²⁵Abstracted from *J. Low-Temp. Phys.* 19(5-6): 493-512 (1975).

²⁶Visiting scientist from AERE, Harwell.

J_c values in magnetic fields up to 70 kOe. Two of the methods (1) resistive measurements and (2) magnetization measurements were carried out in static magnetic fields. The other two methods involved analysis of the response of the sample to a small alternating field superimposed on the static field. The response was analyzed either (3) by measuring the third-harmonic content or (4) by integration of the wave form to obtain a measure of flux penetration. The results are discussed with reference to the agreement between the different techniques and the consistency of the critical state hypothesis on which all these techniques are based. We conclude that flux-penetration measurements by method (4) provide the most detailed information about J_c , but one must be wary of minor failures of the critical state hypothesis. Best results are likely to be obtained by using more than one method.

3.4.2 The Effects of Yttrium or Gadolinium on the Superconducting Transition Temperature of Niobium²⁷ - C. C. Koch and D. M. Kroeger

On quickly cooling from the liquid state during casting, niobium trapped enough yttrium or gadolinium in solid solution to change its physical properties. In particular, the superconducting transition temperature, T_c , was sensitive to small amounts of yttrium or gadolinium in solid solution. Yttrium raised T_c while gadolinium lowered it. When the cast specimens were annealed at temperatures up to 1500°C, the yttrium or gadolinium precipitated and the physical properties reverted to those of pure niobium. Besides T_c , the superconducting critical field, H_{C2} , normal state electrical resistivity, ρ , x-ray lattice parameter, a_0 , and optical and electron microscopy were used to study the Nb-Y and Nb-Gd alloys.

3.4.3 Critical Temperature and Its Pressure Dependence for Technetium-Base HCP Solid-Solution Alloys²⁸ - R. N. Shelton,²⁹ T. F. Smith,²⁹ C. C. Koch, and W. E. Gardner³⁰

The superconducting transition temperature, T_c was determined for a number of technetium-base hcp solid-solution alloys. Additions of V, Nb, and Mo raise T_c , whereas Co, Ni, Ru, and, in particular, Cr and Fe lower T_c relative to pure technetium. The general trend of T_c with the electron per atom ratio is consistent with that expected for a simple dependence on a rigid-band density of states, with the exception of that

²⁷Abstracted from *Philos. Mag.* 30(3): 501-13 (1974).

²⁸Abstracted from paper accepted for publication in *Journal of Physics F: Metal Physics*.

²⁹Institute for Pure and Applied Physical Science, University of California, San Diego, La Jolla, CA 92037.

³⁰Materials Physics Division, AERE, Harwell.

for the chromium and iron alloys. An analysis of the data for these latter alloys in the context of the theory due to Kaiser would suggest that the enhanced depression of T_c is due to the formation of a nonmagnetic resonance state. The hydrostatic pressure dependence of T_c has been investigated up to 25 kbar (2.5 GPa), with particular attention given to the hcp region of the Mo-Tc-Ru system. The observed variation of $\partial T_c / \partial P$ is discussed in relation to current theoretical models.

3.4.4 Superconductivity in the Technetium-Titanium Alloy System³¹ — C. C. Koch

We surveyed superconducting transition temperatures and crystal structures for the technetium-titanium alloy system. The highest transition temperature in this system (10.89 K) occurs in the hcp technetium-rich solid solution. The system is qualitatively similar to the rhenium-titanium system and follows the generally observed dependence of transition temperatures on average group number and crystal structure.

3.4.5 A Study of the Frequency Dependence of AC Losses in Type II Superconductors³² — D. J. Griffiths,³³ C. C. Koch, and J. P. Charlesworth²⁶

As background work for a study of ac losses in Nb₃Sn supported by the Division of Electric Power Transmission and Distribution of the Energy Conservation Administration of ERDA, we have studied the frequency dependence of ac losses.

Energy losses occurring under the application of an alternating magnetic field were examined in type II superconductors representative of three different classes of material: (1) single-crystal niobium (elemental) in the Meissner state, (2) Mo-25 at. % Re (alloy) in fields both below and well above H_{C1} , and (3) Nb₃Sn (compound) principally in the mixed state. Losses were measured as a function of field amplitude and frequency in order to determine whether losses of other than hysteretic were present.

The loss per surface area per cycle had the form $W(h_0, \nu) = W_0(h_0) + \nu f(h_0)$, where $W_0(h_0)$ is identified as hysteretic term, ν is the frequency, and h_0 is the ac field amplitude. Only in the Mo-25 at. % Re alloy did the hysteretic term completely mask the frequency-dependent one. Hysteretic losses in the single-crystal niobium and two Nb₃Sn specimens prepared by different solid-state diffusion methods depended strongly on the degree

³¹Abstracted from paper accepted for publication in *Journal of Less-Common Metals*.

³²Abstract of paper submitted for publication.

³³On sabbatical leave from Physics Department, Oregon State University, Corvallis, Oregon.

of surface roughness (on a scale of about 1 μm). The nonhysteretic losses showed only a mild dependence on the topology of the surface. It is suggested that the frequency-dependent loss per cycle originates from either fluxoid motion or surface scattering of normal excitations.

3.4.6 Work in Progress and in Support of Other Programs — C. C. Koch and D. S. Easton

Studies of the influence of metallurgical structure on fluxoid pinning (critical current density) are in progress in Nb-38 at. % Hf and several titanium-niobium alloys. The Nb-38 at. % Hf samples are of interest because of the marked "peak" effect developed in this system on precipitation of the hafnium-rich alpha phase. The influence of the presence of large yttrium particles on fluxoid pinning is being studied in Ti-Nb alloys where the primary pinning sites are small precipitate particles (omega and/or alpha) and/or dislocation cell walls.

We have also carried on basic research in support of an applied program on stress effects in superconductors, which is funded by the Superconducting Magnet Development Group, Thermonuclear Division, ORNL.

4. RADIATION EFFECTS

J. O. Stiegler and K. Farrell

The Radiation Effects program has as its goal the understanding of the nature and effects of microstructural damage caused by neutrons, with the ultimate objective of controlling or minimizing the damage. The phenomena of swelling and embrittlement are of particular interest. Study of these processes usually requires slow and costly neutron-irradiation experiments and subsequent analyses. However, some aspects of damage can be simulated by the use of energetic ions and electrons that create displacement damage. These simulation techniques complement studies of neutron damage; simulation allows us to examine more variables in shorter times and at less expense. It also permits us to make more efficient use of our neutron irradiations by screening out potentially unsuitable materials. More importantly, the simulation techniques offer approaches for unfolding details of the evolution of damage structures that are difficult to elucidate from neutron experiments. Accordingly, we have expanded our ion and electron irradiations.

The Radiation Effects program receives support from ERDA through the Division of Physical Research, the Reactor Research and Development Division, and the Division of Controlled Thermonuclear Research. We report here only the work sponsored by the Division of Physical Research. Other activities related to reactor applications are covered in reports issued by the appropriate programs.

4.1 THEORY

4.1.1 Diffusion of Point Defects in Irradiated Metals¹ - M. H. Yoo and W. H. Butler

Three-dimensional diffusion of point defects under the influence of a force field is an important process of radiation damage in metals. The diffusion equation including the drift term due to the long-range interaction between the defects and a sink is solved for the steady-state concentration of point defects. The problem can be reduced to solving a system of linear differential equations or, alternatively, solving a system of linear integral equations. The boundary condition at the sink is treated by use of a discrete lattice diffusion model. The effective capture radius of a sink is calculated directly from the flux integral of point defects. Example solutions are presented for vacancy-interstitial recombination, point defect trapping at impurities, and growth of very

¹Abstract of a talk presented at the Spring Meeting of the Metallurgical Society of AIME, Toronto, Canada, May 18-22, 1975. Paper submitted for publication.

small dislocation loops by absorption of point defects. For extended defects, such as dislocation loops, the bias factors for interstitials over vacancies are obtained from the capture radii. Effects of temperature, point defect parameters, and elastic properties of the medium on the kinetics of these defect reactions are analyzed, and applications of the calculated results to the study of radiation-induced void formation are discussed.

4.1.2 Point Defect Diffusion Bias for Finite Dislocation Loops¹ — W. A. Coghlan and M. H. Yoo

The most recent theories for swelling and void growth are based on the supposition that prismatic loops are better sinks than voids for interstitials. We have numerically calculated the diffusion of vacancies and interstitials to finite prismatic dislocation loops in aluminum. The loop is placed in the center of a cylindrical region that has a matrix of initial defect concentrations. The boundary values are determined both at the loop core and the outside boundary of the cylinder, and the diffusion equation is used to determine the change in concentration at each matrix point. The solution is iterated until steady state is reached, and the defect flux is found by integrating over a closed surface around the loop. Steady-state defect fluxes are calculated including and excluding the stress field interaction. The diffusion bias is the ratio of these fluxes. These values are plotted as a function of loop radius in Fig. 4.1. Since a bias of 1.0 means that the diffusion fluxes are not affected by the stress field interaction, the figure shows that the interaction plays an increasingly important role for small loops — especially for interstitials. Although this bias factor depends on the dislocation core radius, the magnitude of the bias for interstitials is larger than that currently being used in void growth models. The calculations show that large loops do not show any appreciable bias. This results from the breakdown of the dilute sink approximation. Large loops grow from point defects produced in a region around them. Work is continuing to include defect production in the region around the loop.

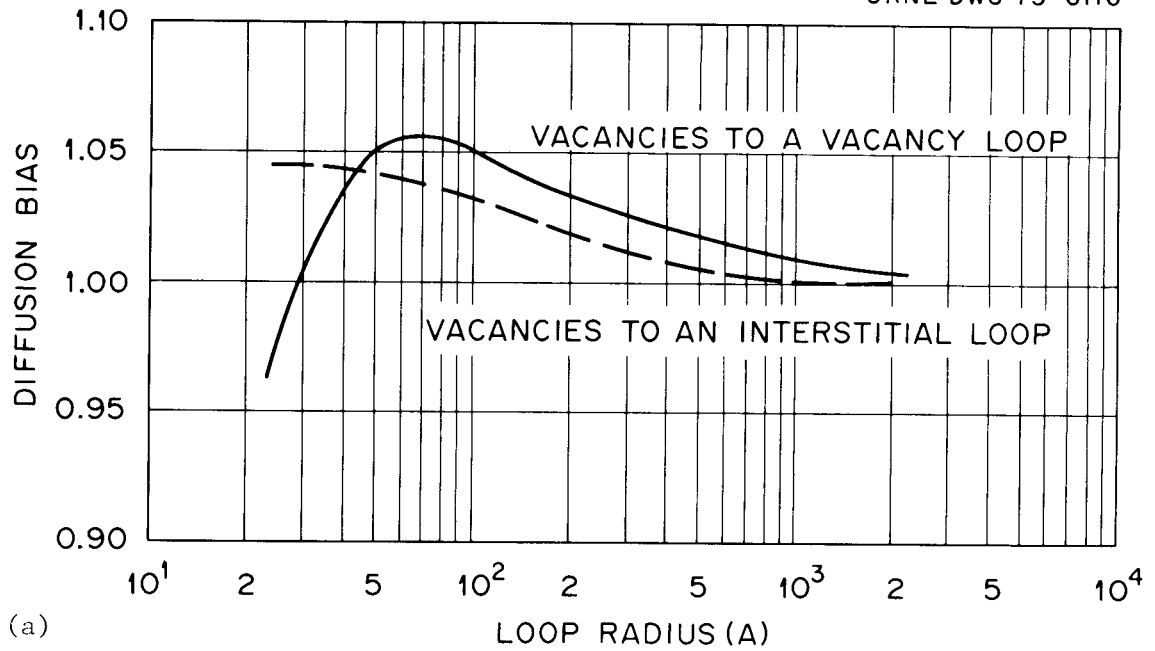
4.1.3 The Climb of Edge Dislocations During Irradiation² — W. G. Wolfer and M. Ashkin³

The steady-state diffusion of radiation-produced point defects in the stress field of an edge dislocation is solved by a perturbation method. The drift term entering the diffusion equation includes the size interaction and the inhomogeneity interaction as well as the effects

²Abstract of paper submitted to *Journal of Applied Physics*.

³On assignment from Westinghouse Research Laboratory, Pittsburgh, Pa. 15235.

ORNL-DWG 75-6116



ORNL-DWG 75-6119

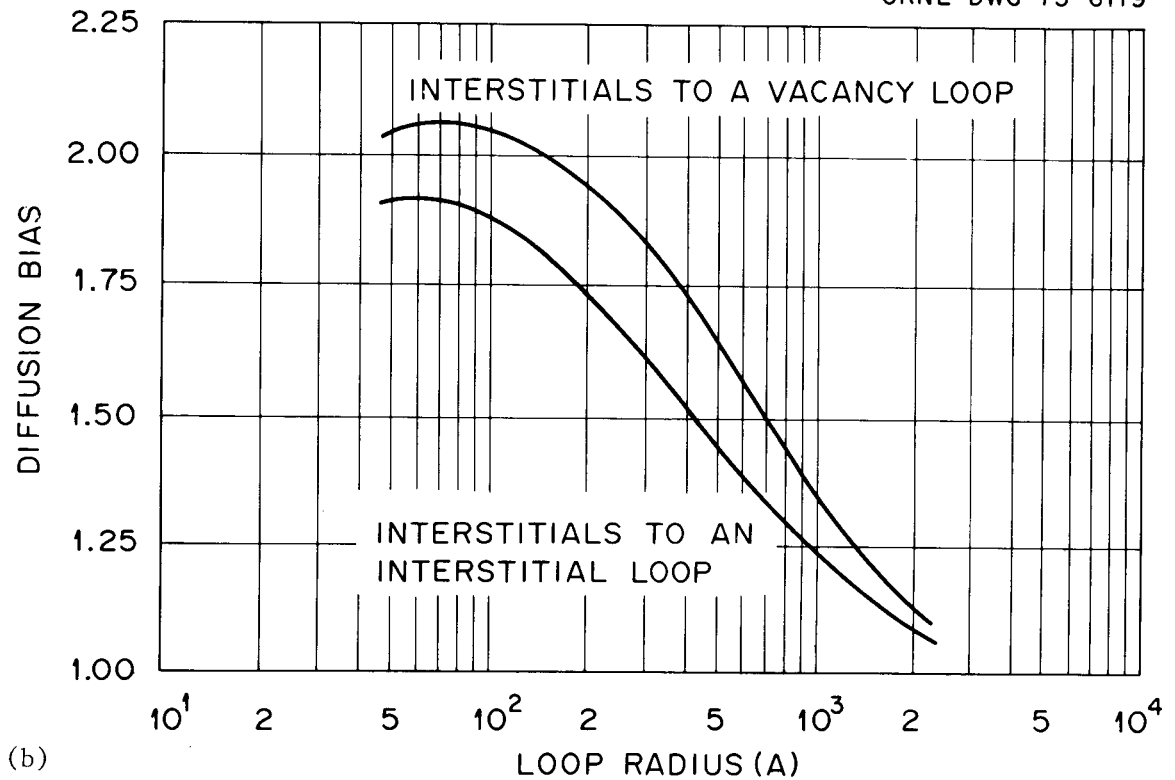


Fig. 4.1. The Diffusion Bias for Point Defects Diffusing to a Prismatic Dislocation Loop in Aluminum as Functions of Loop Radius. (a) Vacancies. (b) Interstitials.

of externally applied stresses. By comparing the perturbation solution with the rigorous solution of Ham, we show that the perturbation solution is always adequate provided the drift term is proportional to the gradient of the interaction energy of the point defect with the dislocation. The steady-state distributions of vacancies and interstitials are such that voids or vacancy clusters preferentially nucleate on the compressive side of the edge dislocation. The external stresses give rise to an orientation-dependent bias of the edge dislocation; this bias is shown to give rise to radiation-induced creep.

4.1.4 Prediction of Irradiation Creep From Microstructural Data⁴ — W. G. Wolfer

Most explanations of irradiation creep are linked to the formation of a new dislocation structure by precipitation of point defects during irradiation. Presently, no quantitative theories can predict the densities of dislocations, loops, and voids as functions of dose; these densities must be measured experimentally, and they can then be used subsequently in theoretical models. This will be done here with a model proposed recently that derives irradiation creep from stress-dependent bias factors. If C and C° denote point defect concentrations and D and D° the diffusivities far away from and at a sink, respectively, then the point defect current to the sink is given by

$$J = AZ(DC - D^\circ C^\circ) , \quad (1)$$

where A is a geometrical factor and Z is a stress-dependent bias factor. The bias factor of a small prismatic interstitial loop of radius R is⁵

$$Z^L = 1 - 0.0335 \frac{\alpha^G}{GbRkT} b_i s_{ij} b_j + \frac{b^2}{R^2} \left[\left(0.024 \frac{vG}{kT} \right)^2 + 3.225 \right. \\ \left. \times 10^{-4} \frac{\alpha^K}{kT} - 3.073 \times 10^{-4} \frac{\alpha^G}{kT} \right] , \quad (2)$$

and the bias factor for an edge dislocation parallel to the unit vector \vec{n} is⁶

⁴Summary of a paper accepted for publication in *Scripta Metallurgica*.

⁵W. G. Wolfer and M. Ashkin, *J. Appl. Phys.* 46: 547 (1975).

⁶W. G. Wolfer and M. Ashkin, to be published.

$$Z^{\perp} = 1 + \frac{b^2}{16a^2 \ln(d/a)} \left[\left(0.197 \frac{vG}{kT} \right)^2 - 0.01654 \frac{\alpha^K}{kT} - 0.1089 \frac{\alpha^G}{kT} - 0.005514 \frac{\alpha^G \sigma_{kk}}{(kT)^2} - \left(0.0224 \frac{\alpha^G}{b^2} b_i b_j + 0.00448 \alpha^G n_i n_j \right) \frac{v s_{ij}}{(kT)^2} \right]. \quad (3)$$

Here, G is the shear modulus, k the Boltzmann constant, T the absolute temperature, \vec{b} the Burgers vector, σ_{kk} the trace of the stress tensor, s_{ij} the deviatoric stress tensor, $a \cong 7b$ (an effective core radius), and $d = 1/\sqrt{\pi\rho}$, the average distance between dislocations with density ρ . Other parameters are the relaxation volume v and the elastic polarizabilities α^K and α^G of the point defects. For interstitials, they are $v_I = 1.4\Omega$ (Ω = atomic volume), $\alpha_I^K = 100$ eV, $\alpha_I^G = -150$ eV, and for vacancies: $v_v = -0.2\Omega$, $\alpha_v^K = -150$ eV, and $\alpha_v^G = -15$ eV. Apart from the stress-dependent bias factors, C° also depends on the stress as $C^\circ \propto \exp(b_i s_{ij} b_j / kT)$. The average concentrations C_I and C_v can be determined from the two rate equations for interstitials and vacancies,⁷ and the defect currents can then be computed from Eq. (1).

To construct a creep model we assume a random distribution of interstitial loops (with density N) and dislocations. Then, the irradiation creep rate is given by

$$\dot{\epsilon}_{ij} = N\Omega \int d\omega_b \left(J_I^{\perp} - J_V^{\perp} \right) b_i b_j + \rho\Omega \int d\omega_n \int d\omega_b \left(J_I^{\perp} - J_v^{\perp} \right) b_i b_j, \quad (4)$$

where the integration is over all orientations of the Burgers vector \vec{b} and, in the case of edge dislocations, also over the orientations of the vectors \vec{n} perpendicular to \vec{b} . It is found that $\dot{\epsilon}_{ij}$ has three contributions, all being linear in s_{ij} , and the third contribution is thermal creep by the Nabarro-Herring mechanism. Using the measured⁸ parameters ρ , N , and R for solution-annealed type 316 stainless steel, $\dot{\epsilon}_{ij}/\sigma_{ij}$ is computed and plotted as a function of $1/T$ in Fig. 4.2. All solid symbols refer to values for fluences around 2×10^{22} n/cm² (>0.1 MeV) or greater, all open symbols to low-fluence data below about 1×10^{22} n/cm². The curves are best fits through the data points. From in-reactor creep measurements, Mosedale et al.⁹ found that in the range 270 to 295°C the steady-state creep rate for solution-annealed type 316 stainless steel gave values for $\dot{\epsilon}/\sigma$ that ranged from 2.3×10^{-15} to 6.6×10^{-15} (sec psi)⁻¹ [3.3×10^{-19} to 9.6×10^{-19} (sec Pa)⁻¹]. The low-fluence data (open symbols) predict a much too low creep rate. However, with the high-fluence data the predicted irradiation creep behavior not only agrees remarkably well with in-reactor

⁷W. G. Wolfer and J. L. Straalsund, *Scr. Metall.* 7: 161 (1973).

⁸H. R. Brager and J. L. Straalsund, *J. Nucl. Mater.* 46: 134 (1973).

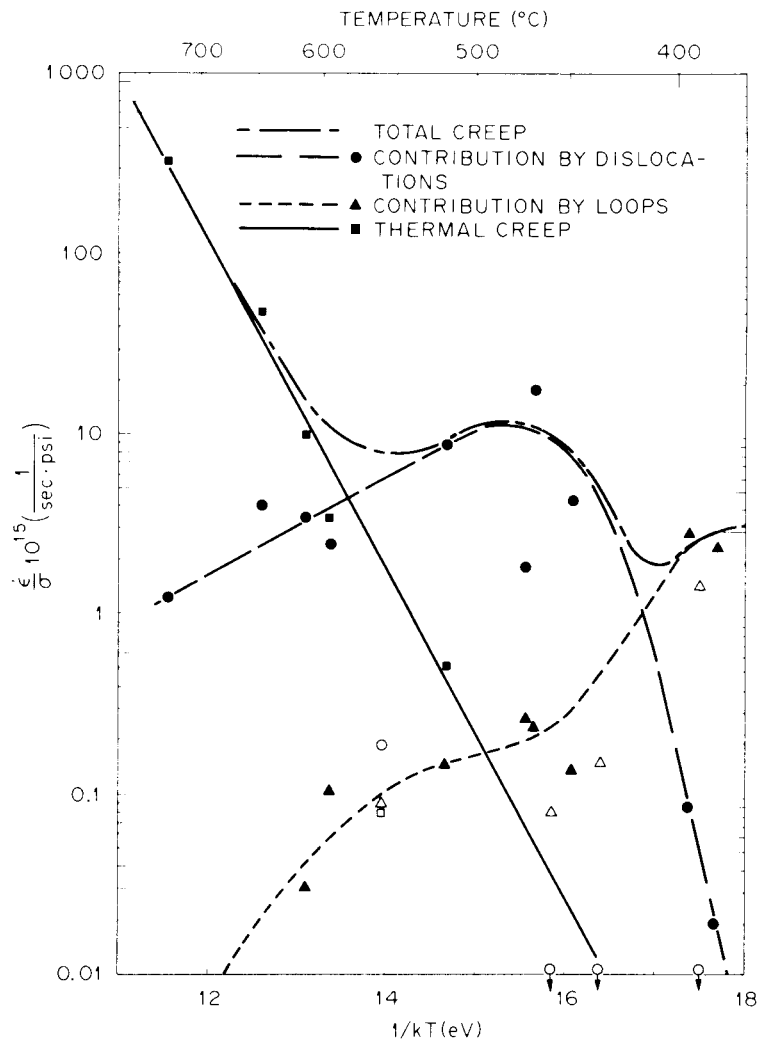


Fig. 4.2. Irradiation Creep Compliance, $\dot{\epsilon}/\sigma$, Versus Reciprocal Temperature. Open symbols, low-fluence ($<1 \times 10^{-22}$ n/cm²) data. Closed symbols, high-fluence (2×10^{-22} n/cm²) data.

measurements,⁹ but the creep rate also increases within the temperature range of swelling in a way not unlike the swelling-enhanced creep observed previously in slit-tube data.¹⁰

⁹D. Mosedale, G. W. Lewthwaite, and I. Ramsey, *Proc. Conf. Irradiation Embrittlement and Creep in Fuel Cladding and Core Components*, British Nuclear Energy Society, London, 1972, p. 233.

¹⁰J. P. Foster, R. V. Strain, and W. G. Wolfer, *Nucl. Engr. Design* 31: 117 (1974).

4.1.5 Comparison of Void Growth Kinetics in Irradiated Stainless Steels and Pure Metals¹¹ - L. K. Mansur, K. Farrell, and J. O. Stiegler

Two models of void growth are examined in terms of a single parameter, Q , the ratio of absorption of point defects at dislocations to that at voids. In the first model to be considered, diffusion of point defects to the void determines growth kinetics,¹²⁻¹⁴ and the ratio can be expressed¹⁵ as

$$Q_D = L/2 \ln(r_s/r_c) \int r n(r) dr . \quad (5)$$

In the second model, growth is determined by the incorporation rate of defects at the void surface,¹⁵ and the ratio is

$$Q_S = Lk_v^d/4\pi k_v^v \int r^2 n(r) dr . \quad (6)$$

Here, L is the dislocation density in cm/cm^3 , $n(r) dr$ is the density (cm^{-3}) of voids of radius r to $(r + dr)$, r_s/r_c is the ratio of the extent of the dislocation diffusion field to the capture radius for vacancies, and k_v^d/k_v^v is a constant.

For temperatures at or below the swelling peak, the dominant kinetics for the diffusion-controlled case are approximated by

$$\bar{r} \propto (\text{dose})^{1/2} / L \quad Q_D \gg 1 , \quad (7)$$

$$\bar{r} \propto L^{1/4} (\text{dose})^{1/4} / N \quad Q_D \ll 1 . \quad (8)$$

¹¹Summary of a talk presented at the 1975 Annual Meeting of the American Nuclear Society, New Orleans, June 8-13, 1975. Published in *Trans. Am. Nucl. Soc.* 21: 167 (June 1975).

¹²A. D. Brailsford and R. Bullough, *Nucl. Metall.* 18: 493 (1973).

¹³S. D. Harkness and Che-Yu Li, *Metall. Trans.* 2: 1457 (1971).

¹⁴H. Wiedersich, *Rad. Eff.* 12: 111 (1972).

¹⁵L. K. Mansur, P. R. Okamoto, A. Taylor, and Che-Yu Li, *Nucl. Metall.* 18: 509 (1973); also, "Surface Reaction Limited Void Growth," presented at the ASTM Gatlinburg Symposium on Radiation Effects on Structural Materials, to be published.

For the surface-limited model,

$$\bar{r} \propto \text{dose}/L \quad Q_S \gg 1, \quad (9)$$

$$\bar{r} \propto L^{1/5} (\text{dose})^{1/5} / N^{2/5} \quad Q_S \ll 1. \quad (10)$$

Thus at $Q_S \ll 1$, swelling is insensitive to void number density, viz. $\Delta V/V \propto N^{-1/5}$.

The appropriate Q values in Table 4.1 are computed for ion- and neutron-irradiated stainless steels^{15,16} as well as for some recent

¹⁶H. R. Brager and J. L. Straalsund, *J. Nucl. Mater.* 46: 134 (1973).

Table 4.1. Values of the Ratio of Point Defect Absorption at Dislocations to that at Voids in Stainless Steels and Pure Metals

Dose	Material	Dislocation Density (cm ⁻²)	Temperature (°C)	Q_S^a	Q_D
<u>Solution-Annealed Stainless Steels^b</u>					
30 dpa (Ni)	Type 304L	1.3×10^{11}	600	29	27.5
100 dpa (Ni)	Type 304L	1.0×10^{11}	600	1.1	4.30
30 dpa (Ni)	Type 304L	2.8×10^{11}	525	28	44.0
100 dpa (Ni)	Type 304L	2.5×10^{11}	525	7.8	17.9
30 dpa (Ni)	Type 316	1.9×10^{11}	525	86	91.8
100 dpa (Ni)	Type 316	2.2×10^{11}	525	12	22.8
2 dpa (electron)	18/8 (1% Si)	1.4×10^{10}	550	1.7	1.68
<u>Solution-Annealed Stainless Steels^c</u>					
2×10^{22} n/cm ²	Type 316	2×10^{11}	390	14	19.5
2×10^{22} n/cm ²	Type 316	2×10^{10}	460	6.2	7.8
4×10^{22} n/cm ²	Type 316	3×10^{11}	390	9.1	21.4
4×10^{22} n/cm ²	Type 316	3×10^{10}	460	1.9	4.3
<u>High-Purity Metals^d</u>					
3.6×10^{19} n/cm ²	99.9999% Al	2.0×10^9	55	0.22	0.15
3.7×10^{20} n/cm ²	99.9999% Al	6.2×10^9	55	0.27	0.33
1.9×10^{21} n/cm ²	99.9999% Al	1.0×10^{10}	55	0.21	0.40
6×10^{20} n/cm ²	Nickel	2.6×10^9	350	0.26	0.26
1×10^{21} n/cm ²	Nickel	3.6×10^9	400	0.37	0.51
9×10^{20} n/cm ²	Nickel	1.8×10^9	450	0.29	0.47
9.6×10^{20} n/cm ²	Nickel	1.3×10^9	500	0.34	0.42
1.2×10^{21} n/cm ²	Nickel	7.1×10^8	550	0.57	0.72

^aThis assumes $k_v^d/4\pi k_v^v$ is about 10^{-7} , as has been shown.^b

^bL. K. Mansur et al., *Nucl. Metall.* 18: 509 (1973).

^cH. R. Brager and J. L. Straalsund, *J. Nucl. Mater.* 46: 134 (1973).

^dK. Farrell, R. W. Chickering, and J. O. Stiegler, ORNL, unpublished.

measurements on neutron-irradiated pure aluminum and pure nickel.¹⁷ Aluminum and nickel have $Q < 1$, while stainless steels have $Q > 1$; therefore, voids in nickel and aluminum should grow approximately according to either Eq. (8) or (10), the slow kinetics equations, depending upon whether diffusion-controlled or surface-limited kinetics applies. For stainless steels, which usually have high Q values, surface-limited kinetics show better agreement with swelling data than do diffusion controlled kinetics. The predictions of the two models in the slow kinetics regime are not very different, but in a detailed analyses of the aluminum data the surface-limited model showed better correlations than did the diffusion-controlled model.

The following conclusions can be drawn:

1. Under the present experimental conditions pure nickel and aluminum swell in the slow kinetics regime; whereas, under conditions of interest to the LMFBR, stainless steels swell in the fast kinetics regime.
2. If this simple analysis is more generally applicable, it may prove useful in forecasting swelling rates at a given temperature from a single set of microstructural measurements.
3. The surface-limited void growth model can be used to predict swelling measurements on pure aluminum as well as stainless steels.
4. For metals where $Q_S < 1$, such as nickel and aluminum, swelling should be insensitive to void number density. As a practical matter, this implies that translation of ion-bombardment to neutron swelling results need not require void nucleation theory to translate expected number densities.

4.2 NEUTRON DAMAGE

4.2.1 Void Nucleation as Inferred from Neutron Irradiations¹⁸ —

E. E. Bloom, K. Farrell, M. H. Yoo, and J. O. Stiegler

A review of the microstructural data available from neutron-irradiated metals suggests the following general conclusions on void nucleation:

1. With few exceptions, low-swelling alloys resist swelling because nucleation does not occur, not because void growth rates are altered relative to other similar alloys.
2. When experimental conditions permit (i.e., low concentrations of voids, loops, and dislocations), nucleation occurs heterogeneously, e.g., in the vicinity of microstructural defects such as dislocations, precipitate particles, and boundaries. At high defect concentrations the correlation between the nucleation site and structural defects is not as clear. The correlation may still exist but may be obscured by the high defect concentration.

¹⁷K. Farrell, R. W. Chickering, and J. O. Stiegler, ORNL, unpublished.

¹⁸Summary of Proceedings of the Consultant Symposium, pp. 330-50 in *Physics of Irradiation Produced Voids*, Harwell, Sept. 9-11, 1974, ed. by R. S. Nelson, AERE-R-7934.

3. Helium may play an even stronger role in the evolution of the irradiation-produced defect structure than previously thought. It may assist the formation of dislocation loops, which provide the bias for subsequent void nucleation and growth. Helium appears to influence nucleation more strongly when present in solution or in small clusters than when present in larger bubbles.

4. Composition, both in terms of major alloying elements and impurities, influences voids nucleation. Limited evidence on aluminum alloys suggests that the development of the dislocation structure is affected in the same direction as the development of the void structure; that is, alloying aluminum increases the incubation fluence for both dislocations and voids.

5. Preirradiation microstructure influences void and loop nucleation, but not always in the same direction in different alloys. This probably reflects differences in dislocation substructure and stability in different metals and alloys.

4.2.2 The Influence of Implanted Helium on the Development of Damage Structure in Neutron-Irradiated Aluminum - K. Farrell, R. W. Chickering,¹⁹ and J. O. Stiegler

High-purity aluminum strips containing an initially uniform distribution of 4 at. ppm of cyclotron-implanted helium were annealed at $0.65T_m$, $0.77T_m$ and $0.96T_m$ to encourage the formation of helium clusters and bubbles. There was no discernable damage from the implantation treatment. A few small bubbles about 50 Å in diameter were found after the $0.96T_m$ anneal but none were visible for lower temperature anneals. There was no measurable loss in helium during annealing. The implanted helium altered the neutron-induced damage structures when there was no prior annealing treatment or when annealing was done below $0.77T_m$ but not when annealing was done at $0.96T_m$. The implanted helium considerably enhanced the formation of voids, and it also significantly encouraged the formation of interstitial loops at fluences below those at which voids were observed. These loops evolved into a dislocation structure that built up faster in the helium-implanted specimens. The onset and the concentration of voids appeared to be connected with the formation and degree of dislocation structure. At the lower fluences the presence of implanted helium increased the level of swelling, but as the fluence increased the swelling values for the nonimplanted specimens approached those for the helium-implanted material. We conclude that a major function of dissolved or clustered helium atoms is to promote the formation of loops and dislocation structure, which provide the biased sinks required for void formation and growth.

¹⁹Summer participant from Purdue University. Now with Westinghouse Advanced Reactors Division, Madison, Pa.

4.2.3 The Effects of Solute Content and Precipitate Distribution on Fast-Neutron Damage in Aluminum-Copper Alloys²⁰ - R. W. Carpenter and J. C. Ogle

Microstructural changes were studied in aluminum-copper alloys containing 1.7 and 3.8 wt % Cu after irradiation to a fluence of about 3×10^{22} cm²/sec (>0.1 MeV) at 55°C. When both alloys were irradiated in the solution-annealed-and-quenched condition (nonrandom solid solution) the 3.8% Cu alloy was the more resistant to swelling. When either alloy was irradiated in an aged condition the differences in damage behavior were less pronounced, but there was a strong dependence of swelling behavior upon precipitate type and distribution in both alloys. All the alloys, whether the preirradiation microstructure was a nonrandom solid solution or multiphase, exhibited less than about 2% swelling, whereas control material of unalloyed aluminum displayed 13% swelling. These results show that the damage resistance of aluminum-copper alloys strongly depends upon composition, but that when precipitation is induced before irradiation, the damage behavior is controlled primarily by the precipitate type and distribution.

4.2.4 Synergistic Effects of Displacement Damage and High Gas Content in Aluminum²¹ - K. Farrell and J. T. Houston

A solid-solution alloy of 2300 at. ppm ⁶Li in aluminum was irradiated at $0.37T_m$ in high fast and thermal fluxes to produce a damage level of about 2 dpa and to simultaneously induce a gas content of about 2200 at. ppm each of ⁴He and ³H from burnup of the ⁶Li. The gases significantly altered the damage structure but did not increase swelling. Lithium-free aluminum contained 1×10^{14} cavities/cm³ of average size about 500 Å, whereas the alloy contained more than 5×10^{16} cavities/cm³ of average size about 50 Å. Additionally, the grain boundaries in the alloy were covered with large cavities. The cavities in the alloy resisted annealing, indicating that they were gas filled. The alloy displayed much more irradiation hardening than the pure aluminum, and when tested in bending at 25 and -196°C it fractured along grain boundaries with no measurable strain. Fractographic examination revealed that between 50 and 90% of the grain boundary area became separated by interlocking gas bubbles during irradiation, and failure during testing occurred by tearing of the remaining portions of intact grain boundaries. We conclude that large gas contents considerably reduce the temperature at which gas bubbles develop and also cause refinement of damage structure. The associated increase in hardness and the weakening of grain boundaries by bubbles lead to severe embrittlement even at low temperatures.

²⁰Abstract of paper to be presented at the International Conference on Fundamental Aspects of Radiation Damage in Metals, Gatlinburg, Tenn., October 5-12, 1975.

²¹Abstract of paper to be presented at the International Conference on Radiation Effects and Tritium Technology for Fusion Reactors, Gatlinburg, Tenn., October 1-3, 1975.

4.2.5 Neutron Damage in Zirconium - K. Farrell

Zirconium is one of the few pure metals that seem to have good resistance to void formation during neutron irradiation. Examination of a number of grades of zirconium irradiated in the Oak Ridge Research Reactor at 450°C to 1 to 2 dpa has, however, revealed the presence of cavities when the zirconium contained helium.

Some of the materials were doped with small quantities of ^{10}B to generate helium during irradiation. There was a coarse structure of neutron-induced dislocations and loops in all materials. The loops were large, 200 to 5000 Å in diameter, and lay in roughly parallel bands each about 1 μm wide with a spacing of about 0.5 μm. The arrangement was similar to but coarser than the aligned loops on prism planes in directions parallel to traces of basal planes that have been reported by others for lower irradiation temperatures. Some of the loops in at least one of the materials displayed fringes reminiscent of stacking faults. The banding of loops was particularly apparent in material containing an estimated 40 at. ppm He from burnup of ^{10}B . Cavities were present and were segregated within the bands of loops. Occasionally, cavities were found on grain boundaries at the junctions of the bands with the boundaries. Materials that did not contain deliberately added ^{10}B but contained measurable natural boron had a few cavities. In one material of small grain size the cavities and loops were both randomly distributed. The incidence of cavities increased markedly with increasing boron content, and the amount of helium calculated to be present is of the order required to stabilize the cavities as equilibrium gas bubbles. A specimen containing hundreds of parts per million of ^{10}B was crammed with gas bubbles, especially large ones on grain boundaries, and showed some evidence of alignment of bubbles within the grains.

4.3 DAMAGE SIMULATION

4.3.1 Improvements to the ORNL Heavy-Ion Bombardment Facility -

N. H. Packan, E. A. Kenik, A. F. Rowcliffe, M. J. Saltmarsh,²²
G. F. Wells,²² C. H. Johnson,²² F. A. McGowan,²² and M. B. Lewis

The past year has seen a succession of significant improvements to the 5-MV Ion Bombardment Facility. Taken together, the changes have permitted the usable beam intensity to be increased by more than a factor of 5 to the present capability of 1.5 μA of 4 MeV Ni^{2+} ions. Simultaneously the spatial uniformity of the beam and the dependability of the system have been improved. Among the major modifications, roughly in the order of their accomplishment, are the following:

1. a changeover from an aluminum source to a nickel source;
2. the addition of a 90° analyzing bending magnet to permit the selection of a chemically pure beam;

²²Physics Division.

3. installation of new coils in the 90° magnet (raising its mass-energy capability to 62 amu-MeV) to permit the use of Ni²⁺ ions rather than the less numerous Ni³⁺;
4. design and installation of a new gas stripper just above the 90° magnet to generate 2+ and higher charge states from the singly charged beam that emerges from the accelerator (the prominent feature of this design is the use of differential pumping at both ends of the stripper tube to minimize any consequent degradation of the beam line vacuum);
5. use in the ion source of separated ⁵⁸Ni powder, obtained from Isotopes Division, in place of natural nickel, which is approximately two-thirds ⁵⁸Ni and one-third ⁶⁰Ni (this change yielded an immediate 50% increase in beam current at the exit of the analyzing magnet);
6. design and installation of a unique "ring lens" that reshapes and improves the uniformity and intensity of the beam at the plane of the specimens;
7. installation of a digitized beam profile monitor to monitor continuously and portray the beam intensity profile during an irradiation run;
8. measurement and accommodation of beam heating at the specimen surface.

A number of further modifications that are now in advanced planning or construction stages are:

1. A getter-ion pump will be installed in the van de Graaff high-voltage terminal to allow generation of a more intense beam and to increase the source lifetime.

2. A new and more versatile damage chamber will be capable of handling up to six sets of specimens before the vacuum needs to be broken to change out the specimens. Specimens will be heated from the back with an electron beam, and the temperature at the bombardment surface will be measured with an infrared thermometer.

3. Improved beam diagnostic apparatus will include a deep Faraday cup and an additional multiscaling current digitizer, which will register the ion dose received by individual specimens.

4.3.2 A Method for Doping Irradiation Samples with Helium Using ²⁴⁴Cm — W. A. Coghlan, N. H. Packan, M. J. Saltmarsh,²² and H. L. Adair²³

The presence of gas atoms, particularly transmutation products such as hydrogen and helium, plays an important role in determining the nucleation and growth of small dislocation loops and voids. We have developed a method using ²⁴⁴Cm for implanting helium atoms in foils that are to be used as targets for heavy-ion radiation damage simulation studies. In the past the implantation has been done with accelerators, but this method is expensive and for a given energy the helium atoms are distributed over a very narrow range of depth; to get a reasonably flat helium construction profile the beam energy must be changed or the sample must be rocked in a carefully prescribed manner. None of these has been entirely satisfactory. The distribution of the atoms is not uniform, and the amount of helium deposited is not known very accurately.

²³Isotopes Division.

The method we have developed using the alpha-particles from ^{244}Cm decay overcomes most of these problems. Theoretically we have shown that if a thin layer of Cm_2O_3 (4-6 μm thick) deposited on a backing material is used as a source of alpha-particles, the deposited helium atoms lie in a uniform concentration to a depth of about 6 μm in Ni. After that depth the concentration decreases linearly to zero at a depth of 12 μm . The extent and uniformity of the flat-concentration region depend on the thickness and uniformity of the Cm_2O_3 film produced. We have had such a film prepared and have implanted helium ions in a number of test specimens. The profile of the helium has not yet been measured, but the average concentration in a 12.5- μm foil has been compared with theoretical predictions. The calculated average and the measured values differ by a few parts per million, which is as good as we can expect from the uncertain physical parameters used in the calculations. Encouraged by our first attempts, we are preparing better characterized sources and will attempt to have the helium concentration profile measured as a function of distance into the foil.

4.3.3 Current Nickel Ion Bombardment Experiments - N. H. Packan, L. K. Mansur, E. A. Kenik, R. W. Carpenter, and K. Farrell

Ion bombardment provides a rapid and inexpensive means of screening prospective reactor materials for swelling resistance. Under suitable conditions swelling is manifest as surface relief, which can be measured with a sensitive profilometer. Our Reactor Materials Group is using the facility for this purpose and has identified some highly promising constructional materials. Likewise, the Damage Mechanisms Group is screening candidate research materials to select those best suited to needs and to check out results reported from other sources. In this latter respect, we have reproduced some previously unconfirmed data on the swelling response of a wide range of Fe-Cr-Ni alloys. Some specific experiments we are performing with the ion facility include a correlation of ion and neutron microstructural damage in pure nickel and a measurement of the temperature shift caused by the higher damage rates in ion bombardment; this work is close to completion. Since the damage region in ion bombardment occurs close ($\approx 0.7 \mu\text{m}$) to the specimen surface we are looking into the questions of whether the damage is influenced by the condition of the surface and by impurities, particularly hydrogen, picked up through the surface. The usual surface preparation is mechanical polishing. Experiments we have made on some Fe-Cr-Ni alloys that had been annealed after mechanical polishing show significantly more swelling than found in as-polished material. With regard to hydrogen, we have very recently implanted some Fe-Cr-Ni alloys and some stainless steels with protons before ion bombardment. These particular specimens showed a wide scatter in swelling response and no conclusive effect of hydrogen. Investigations of surface preparation techniques are continuing in an effort to find the most satisfactory, artifact-free condition. Recently we began experiments designed to study the evolution of dislocation structure in materials of widely different swelling response.

4.3.4 The ORNL Irradiation Creep Facility — T. C. Reiley and E. E. Bloom

Our creep-testing procedure uses thin sheet specimens bombarded by 60-MeV alpha particles from the Oak Ridge Isochronous Cyclotron. These alpha particles pass completely through the specimen, losing only about 10% of their energy in the specimens. Maximum atomic displacement rates calculated for obtainable beam currents correspond closely to displacement rates for EBR-II. The range of test temperatures extends from 300 to 700°C. Temperatures are attained by electrical self-resistance heating and are controlled electronically by monitors that sense small changes in electrical resistance. Experiments have demonstrated that the temperature may be controlled under actual operating conditions to within 0.1°C. The circuit can compensate for a total loss in alpha beam current and will return the specimen to the specified temperature within 1 to 3 sec. The specimen thermal time constant is only about 0.4 sec, which allows rapid corrections to the test temperature. Temperature gradients along the specimen gage length are monitored by infrared pyrometry. The specimen is rapidly cooled by a liquid-nitrogen-filled cooling block placed close to the back of the specimen. The heat conduction medium is helium gas maintained at atmospheric pressure. Ambient temperature control of the apparatus is maintained by circulation of water at constant temperature through each structural member. Specimens can be loaded to stresses up to 345 MPa (50 ksi), and the stress can be changed rapidly. Elongations will be measured by use of two capacitance transducers, one on each side of the specimen. They are shielded from the hot specimen, and their resolution is specified at better than 25 nm (1 microinch). The alpha beam current will be continuously monitored by parallel-plate plasma conduction sensors incorporated into the beam masking arrangement. Beam wobbling will be used to maintain beam uniformity. Effects of high damage levels will be determined on specimens previously irradiated in EBR-II to various displacement levels, some in stressed conditions.

4.3.5 The ORNL High-Voltage Electron Microscope Facility — R. W. Carpenter and E. A. Kenik

The high-voltage electron microscope (HVEM) has been successfully upgraded to operate at a maximum accelerating potential of 1 MeV, from its former limit of 650 keV. Calibration of the electron beam current available at 1 MeV has shown that a maximum of about 21 A/cm² can be attained at the specimen. We are attempting to improve the vacuum at the specimen stage to minimize specimen contamination during HVEM irradiations at elevated temperatures. Our program of HVEM irradiations is still in its infancy. Unlike other HVEM facilities we do not soon intend to use the microscope as a tool for rapidly producing voids and reaching high swelling levels. Rather, we plan to study the relatively neglected area of development of dislocation structures leading to void formation. Our initial experiments on copper implanted with about 14 at. ppm He show that at 250°C during HVEM irradiation, dislocations nucleate at least 20 times as fast as in helium-free copper. There are corresponding

increases in the void nucleation rate and in the degree of swelling. These studies are being pursued at other temperatures to elucidate the role of helium. Other studies will include the effects of minor elements on damage evolution in stainless steels, and the influences of degree of chemical order and of precipitation on damage generated in selected binary alloys systems based on nickel. Critical analyses of the damage produced with the HVEM will be facilitated by postirradiation studies in our new high-resolution JEOLCO model 100C microscope.

APPENDIX

1. STAFF ASSIGNMENTS

C. J. Sparks, Jr., AERE, Harwell, England, September 1973–September 1974.

C. S. Yust, Institut für Reaktorwerkstoffe, KFA, Jülich, Germany, 1 September 1973–1 September 1974.

G. S. Painter, Institut für Festkörperforschung, KFA, Jülich, Germany; H. H. Wills, Physics Laboratory, University of Bristol, England, June 1974–September 1975.

R. A. Vandermeer, Visiting Professor of Material Science, University of Rochester, September 1974–May 1975.

D. L. McElroy, AERE, Harwell, September 1974–September 1975.

D. M. Kroeger, Institut für Festkörperforschung, KFA, Jülich, Germany, September 1974–September 1975.

T. S. Lundy, ORNL, Planning and Analysis Group, October 1974–October 1975.

2. GUEST ASSIGNMENTS

J. P. Charlesworth, AERE, Harwell, England, September 1973–November 1974.

H. Ullmaier, Institut für Festkörperforschung, KFA, Jülich, Germany, January 1974–November 1974.

G. Shankle, Angelo (Texas) State University, ORAU Research Participant, Summer 1974.

D. J. Griffiths, Oregon State University, September 1974–September 1975.

J. Schelten, Institut für Festkörperforschung, KFA, Jülich, Germany, November 1973–November 1974.

H. P. Krautwasser, Institut für Reaktorwerkstoffe, KFA, Jülich, Germany, May 1975–May 1976.

G. Bauer, Institut für Festkörperforschung, KFA, Jülich, Germany, March 1975–March 1976.

- R. Chickering, Purdue University, Summer 1974.
- L. B. Shaffer, Anderson (Indiana) College, Summer 1974.
- O. C. Sartain, Indiana State University, Summer 1975.
- P. L. Leath, Rutgers University, Summer 1975.
- R. Bayuzick, Vanderbilt University, Summer 1975.
- H. Eaton, Vanderbilt University, Summer 1975.
- R. W. Gould, University of Florida, Summer 1975.
- W. Oliver, University of Tennessee, Summer 1975.
- D. G. Dunmire, Thiel (Pennsylvania) College, Summer 1975.
- J. T. Stanley, Arizona State University, Summer 1975.
- B. Gyorffy, H. H. Wills, Physics Laboratory, University of Bristol, Summer 1974, 1975.

3. ORNL-UT JOINT APPOINTMENTS FOR ACADEMIC YEAR 1974-1975

- B. S. Borie, Professor, Metallurgical Engineering.
- C. J. McHargue, Professor, Metallurgical Engineering.
- W. A. Coghlan, Assistant Professor, Metallurgical Engineering.
- G. P. Smith, Professor, Chemistry.

4. PRESENTATIONS AT TECHNICAL MEETINGS - Compiled by Stephanie Davison

78th National Meeting of the American Institute of Chemical Engineers
Session on "Materials Engineering in Nuclear Power Production," Salt
Lake City, Utah, August 18-21, 1974

C. J. McHargue, "Panel on Fusion Reactor Materials and Fuels"

8th International Congress on Electron Microscopy, Canberra, Australia,
August 25-31, 1974

C.K.H. DuBose, G. L. Copeland, and K.H.G. Ashbee, "Transmission
Electron Microscopy of Radioactive Powders"

American Crystallographic Association, Pennsylvania State University,
University Park, Pennsylvania, August 1974

R. W. Hendricks and J. Schelten, "A Pin-Hole Small-Angle X-Ray
Collimation System Using a Position-Sensitive Proportional"

- H. L. Yakel, "The Crystal Structure of a Boron-Rich Boron Carbide"
The Sixth Annual Conference on Surface Studies, Oak Ridge Y-12 Plant,
Oak Ridge, Tennessee, September 10-12, 1974
- R. E. Clausing and R. J. Colchin, "Some Observations on the
Cleanliness and Cleaning of Sputtered Gold Films"
The International Mineralogical Association, 9th General Meeting, West
Berlin, Germany, September 12-18, 1974
- Edwin Roedder and Otto C. Kopp, "An Independent Check on the Validity
of the Pressure Correction in Inclusion Geothermometry, Using
Hydrothermally Grown Quartz"
Bilateral Fast Reactor Exchange Meeting on Fuel Cladding and Core
Structural Alloys Held at AERE Didcot, Berkshire, England, September 16-18,
1974
- Radiation Effects Group, "ORNL Contribution to the USAEC/UKAEA
Bilateral Fast Reactor Exchange Meeting on Fuel Cladding and Core
Structural Alloys"
1974 Fall Meeting of the AIME Symposium on "The Influence of Stresses
and Mechanical Properties of Oxide Scales on the Oxidation Behavior of
Metals," Detroit, Michigan, October 21-24, 1974
- R. W. Carpenter, "Surface Controlled Oxygen Absorption: Kinetics
and Gradients"
J. V. Cathcart, "Mechanisms of Stress Generation and Relaxation
During the Oxidation of U Alloys"
R. E. Pawel and J. J. Campbell, "Some Oxidation Characteristics
of Ta-10 W and Ta-10-W 2.5 Hf Alloys"
Annual Meeting of FACSS, Atlantic City, New Jersey, November 18-22, 1974
- R. E. Clausing and E. E. Bloom, "Auger Electron Spectroscopy of
Fracture Surfaces in Irradiated Type 304 Stainless Steel"
Fall Meeting of the American Physical Society, Atlanta, Georgia,
December 5-7, 1974
- W. H. Butler, "Multiple Scattering Theory for Weak Scatterers:
Application to Al"
4th Annual Symposium on Applied Vacuum Science and Technology, Tampa,
Florida, February 21, 1975
- T. C. Reiley, "Deposition Profiles from Electron Beam-Heated
Evaporation Sources"
American Crystallographic Association Meeting at the University of
Virginia, Charlottesville, Virginia, March 9-13, 1975
- C. J. Sparks, Jr. and J. B. Hastings, "X-Ray Diffraction and
Fluorescence at the Stanford Synchrotron Radiation Project" (invited
paper)

1975 Particle Accelerator Conference, Washington, D. C., March 12-14, 1975

C. J. McHargue, "The Use of Accelerators to Study Irradiation Effects"

Warwick Surface Science Conference, Warwick, England, March 17-20, 1975

R. O. Jones, P. J. Jennings, and G. S. Painter, "Cluster Calculations of the Electronic Structure of Transition Metal Surfaces"

Conference on Study of Carbon and Graphite by Electron Microscope Methods, University College of Wales, Aberystwyth, Wales, March 24-26, 1975

C. S. Yust, E. Pollmann, and P. Krautwasser, "Transmission Electron Microscopy of Pyrolytic Carbon Coatings"

Denver Meeting of the American Physical Society, Denver, Colorado, March 31-April 3, 1975

W. H. Butler, "A One-Dimensional Model of a Transition Metal Alloy"

J. S. Faulkner, "Electronic States of Sub-Stoichiometric PdH"

J. J. Olson, "Comment on the Anderson-McMillan Prescription for the Density of States of Liquid Iron"

American Physical Society Meeting, Washington, D. C., April 28-May 1, 1975

D. J. Griffiths, C. C. Koch, and J. P. Charlesworth, "Evidence of Non-Hysteretic A.C. Losses in Nb₃Sn"

J. D. McGervey, V. W. Lindberg, and R. W. Hendricks, "Positron Trapping in Voids in Aluminum"

AIME Spring Meeting, Toronto, May 1975

W. A. Coghlan and M. H. Yoo, "A Calculation of the Diffusion Bias for Prismatic Dislocation Loops"

D. S. Easton and C. C. Koch, "Tensile Properties of Superconducting Composite Conductors and Nb-Ti Alloys at 4.2 K"

T. C. Reiley and W. D. Nix, "The Structure and Mechanical Properties of Physical Vapor Deposited Chromium"

R. A. Vandermeer, "Aging Induced Shape Instability in an Elastically Bent Uranium + 7.5 wt % Niobium + 2.5 wt % Zirconium Alloy"

C. L. White and D. F. Stein, "Theoretical Aspects of Solute Segregation to Grain Boundaries"

M. H. Yoo and W. H. Butler, "A Steady State Solution to the Diffusion Equation for Point Defects Including the Interaction Force Field"

14th International Conference on Thermal Conductivity, University of Connecticut, Storrs, Connecticut, June 2-4, 1975

J. P. Moore, R. S. Graves, M. B. Herskovitz, K. R. Carr, and R. A. Vandermeer, "Nicrosil II and Nisil Thermocouple Alloys: Physical Properties and Behavior During Thermal Cycling to 1200 K"

1975 Annual Meeting of the American Nuclear Society, New Orleans, Louisiana, June 8-13, 1975

L. K. Mansur, K. Farrell, and J. O. Stiegler, "Comparison of Void Growth Kinetics in Irradiated Steels and Pure Metals"

International Conference on Radiation Damage in Metals

W. G. Wolfer, "Segregation of Vacancies and Interstitials by Internal Stress Fields"

International Discussion Meeting on Flux Pinning in Superconductors

C. C. Koch and D. M. Kroeger, "Fluxoid-Pinning in Niobium Containing Small Amounts of Yttrium or Gadolinium"

5. PUBLICATIONS - Compiled by Judy Young

J. B. Bates, R. W. Hendricks, and L. B. Shaffer, "Neutron Irradiation Effects and Structure of Noncrystalline SiO₂," *J. Chem. Phys.* 61(10): 4163-76 (November 1974).

E. E. Bloom, J. M. Leitnaker, and J. O. Stiegler, *Effect of Neutron Irradiation on the Microstructure and Properties of Titanium Stabilized Type 316 Stainless Steels*, ORNL-TM-4731 (January 1975).

P. T. Carlson, *MATANO - A Computer Code for the Analysis of Interdiffusion and Intrinsic Diffusion Information in Binary Systems*, ORNL-5045 (June 1975).

P. T. Carlson, M. A. Dayananda, and R. E. Grace, "Atomic Mobilities and Vacancy Wind Effects for Diffusion in Ternary Silver-Zinc-Cadmium Solid Solutions," *Metall. Trans.* 6A(6): 1245-52 (June 1975).

J. V. Cathcart, R. E. Pawel, and G. F. Petersen, "High Temperature Oxidation of Uranium Alloys," pp. 669-74 in *Proc. 5th Intern. Congr. Metallic Corrosion*, National Association of Corrosion Engineers, Houston, Texas, 1974.

B. Chakravarti, E. A. Starke, Jr., C. J. Sparks, and R. O. Williams, "Short Range Order and the Development of Long Range Order in Ni₄Mo," *J. Phys. Chem. Solids* 35(9): 1317-25 (September 1974).

R. E. Clausing, C. J. McHargue, and J. E. Spruiell, "Some Remarks on the Importance of Contaminants in High Temperature Applications of Niobium and Vanadium," pp. 123-24 in *Surface Effects in Controlled Fusion* (Proc. Conf. Surface Effects in Controlled Thermonuclear Fusion Devices and Reactors, Argonne, Illinois, USA, 10-12 January 1974) ed. by H. Wiedersich, M. S. Kamisky, and K. M. Zwilsky, North Holland Publishing Company, Amsterdam.

D. S. Easton, C. C. Koch, D. M. Kroeger, and J. W. Cable, "Superconducting Transition Temperatures of Chemically Vapour Deposited Tungsten-Rhenium Alloys," *Philos. Mag.* 30(5): 1117-34 (November 1974).

J. E. Epperson, R. W. Hendricks, and K. Farrell, "Studies in Voids in Neutron Irradiated Aluminum Single Crystals. I. Small-Angle X-Ray Scattering and Transmission Electron Microscopy," *Philos. Mag.* 30(4): 803-17 (October 1974).

C. B. Finch, G. W. Clark, L. A. Harris, and C. S. Yust, "Czochralski Growth and Characterization of Single-Crystal Akermanite ($\text{Ca}_2\text{MgSi}_2\text{O}_7$)," *J. Cryst. Growth* 23: 295-98 (1974).

R. W. Hendricks, J. Schelten, and W. Schmatz, "Studies of Voids in Neutron Irradiated Aluminum Single Crystals. II. Small-Angle Neutron Scattering," *Philos. Mag.* 30(4): 819-37 (October 1974).

R. W. Hendricks, P. G. Mardon, and L. B. Shaffer, "The X-Ray Zero-Angle Scattering Cross Section of Water," *J. Chem. Phys.* 61(1): 319-22 (July 1974).

J. D. Holder and B. F. Oliver, "The Directional Solidification of Pb-Sn-Cd Alloys," *Metall. Trans.* 5(11): 2423-37 (November 1974).

S. H. Jury, D. Arnurius, T. G. Godfrey, D. L. McElroy, and J. P. Moore, "End Effects on the Flow of Heat, Mass or Electrical Energy Through Cylindrical Rod," *J. Franklin Inst.* 298(3): 151-79 (September 1974).

C. C. Koch and D. M. Kroeger, "The Effects of Yttrium or Gadolinium on the Superconducting Transition Temperature of Niobium," *J. Less-Common Met.* 40(3): 29-38 (March 1975).

C. C. Koch and D. M. Kroeger, "Fluxoid Pinning in Niobium Containing Small Amounts of Yttrium or Gadolinium," *Philos. Mag.* 30(3): 501-13 (September 1974).

C. C. Koch, W. E. Gardner, and M. J. Mortimer, "The Effects of Some 3d and 4d Solutes on the Superconductivity of Technetium," pp. 595-600 in *Low Temperature Physics-LT13, Volume 2: Quantum Crystals and Magnetism* (Proc. XIIIth Int. Conf. Low Temperature Physics, Boulder, Colo., Aug. 21-25, 1972) Plenum, New York, 1974.

Thomas G. Kollie, D. L. McElroy, J. T. Hutton, and W. M. Ewing, "A Computer-Operated Fused Quartz Differential Dilatometer," pp. 129-46 in *Thermal Expansion - 1973 (Lake of the Ozarks)*, AIP Conf. Proc. 17, eds. by R. E. Taylor and G. L. Denman, American Institute of Physics, New York, 1974.

D. M. Kroeger, C. C. Koch, and J. P. Charlesworth, "A Comparison of Methods for Measuring Flux Gradients in Type-II Superconductors," *J. Low Temp. Phys.* 19(5/6): 493-512 (June 1975).

J. M. Leitnaker and J. O. Stiegler, "Comment on Ashbee *Et Al*'s Paper on Voids in Boron Carbide," *J. Nucl. Mater.* 55(1): 113-16 (January 1975).

L. K. Mansur, K. Farrell, and J. O. Stiegler, "Comparison of Void Growth Kinetics in Irradiated Stainless Steels and Pure Metals," (Summary) *Trans. Am. Nucl. Soc.* 21(TANSAO 21): 163-64 (June 1975).

C. J. McHargue, "The Use of Accelerators to Study Irradiation Effects," *IEEE Trans. Nucl. Sci.* NS22: 1743-48 (June 1975).

C. J. McHargue, Chaps. 2 and 3 in *Report of the AdHoc Panel on the Use of Accelerators to Study Irradiation Effects*, Committee on Nuclear Science, National Research Council, National Academy of Sciences, Washington, 1974.

J. P. Moore, R. K. Williams, and R. S. Graves, *Lattice Thermal Conductivities of RbBr, RbI, and RbCl From 80 to 400 K*, ORNL-TM-4797 (April 1975).

J. P. Moore, R. K. Williams, and R. S. Graves, "Lattice Thermal Conductivities of RbBr, RbI, and RbCl From 80 to 400 K," *Phys. Rev.* 11(8): 3107-115 (April 1975).

J. P. Moore, D. L. McElroy, and R. S. Graves, *Technique for Determining Thermal and Electrical Conductivity and Absolute Seebeck Coefficient Between 300 and 1000 K*, ORNL-4986 (September 1974).

H. K. Peterson, L. M. Schwartz, and W. H. Butler, "Short-Range Order and the Electronic Structure of a One-Dimensional Liquid Metal," *Phys. Rev. B* 11(10): 3678-86 (May 1975).

G. L. Powell, R. E. Clausing, and G. E. McGuire, "Sodium Segregation onto a Lithium Metal Surface," *Surf. Sci.* 49(1): 310-14 (Apr. 1, 1975).

G. L. Powell, G. E. McGuire, D. S. Easton, and R. E. Clausing, "Auger Spectra of Lithium Hydride," *Surf. Sci.* 46(2): 345-57 (December 1974).

Cullie J. Sparks, Jr., "Inelastic Resonance Emission of X Rays: Anomalous Scattering Associated with Anomalous Dispersion," *Phys. Rev. Lett.* 33(5): 262-65 (July 1974).

C. J. Sparks, Jr. and J. C. Ogle, "Quantitative Trace Element Analysis with X-Ray Fluorescence," pp. 421-39 in *Proc. 1st Annu. NSF Trace Contaminants Conf.*, CONF-730802 (March 1974).

P. A. Staats and O. C. Kopp, "Studies on the Origin of the 3400 cm^{-1} Region Infrared Bands of Synthetic and Natural α -Quartz," *J. Phys. Chem. Solids* 35(9): 1029-33 (September 1974).

R. A. Weeks, J. C. Pigg, and C. B. Finch, "Charge-Transfer Spectra of Fe^{8+} and Mn^{2+} in Synthetic Forsterite (Mg_2SiO_4)," *Am. Mineral.* 59(11-12): 1259-66 (November-December 1974).

R. K. Williams, "A Study of the Electrical Resistivity of Zone-Refined Tungsten at High Temperatures," *J. Appl. Phys.* 46(2): 475-90 (February 1975).

R. O. Williams, "The Nature of the Limitations of Second Law Determinations of Solution Thermodynamics," *Mater. Sci. Eng.* 19(1): 37-42 (May 1975).

R. O. Williams, "Short Range Order Structure in a Copper 16 Atomic Percent Aluminum Alloy," *Metall. Trans.* 5(8): 1843-50 (August 1974).

A. Wolfenden and M. H. Yoo, "Electron Irradiation Damage in Titanium," *Radiat. Eff.* 22(1): 67-70 (May 1974).

M. H. Yoo, "Suppression of Void Formation in Zirconium," pp. 297-307 in *Zirconium in Nuclear Applications, ASTM Spec. Tech. Publ.* 551, American Society for Testing and Materials, Philadelphia, 1974.

C. S. Yust and H. P. Krautwasser, "Transmission Electron Microscopy of Propene-Derived Pyrolytic Carbon Coatings," *Carbon* 13(2): 125-33 (April 1975).

INTERNAL DISTRIBUTION

- | | |
|------------------------------------|------------------------------------|
| 1-3. Central Research Library | 41. H. E. McCoy |
| 4. ORNL - Y-12 Technical Library | 42. H. F. McDuffie |
| Document Reference Section | 43. D. L. McElroy |
| 5-9. Laboratory Records Department | 44-63. C. J. McHargue |
| 10. Laboratory Records, ORNL RC | 64. P. Patriarca |
| 11. ORNL Patent Office | 65. H. Postma |
| 12. G. M. Adamson, Jr. | 66. C. R. Richmond |
| 13. S. E. Beall | 67. M. W. Rosenthal |
| 14. D. S. Billington | 68. J. L. Scott |
| 15. B. S. Borie | 69. D. Steiner |
| 16. J. Brynestad | 70. P. H. Stelson |
| 17. F. R. Bruce | 71. J. O. Stiegler |
| 18. J. V. Cathcart | 72. D. B. Trauger |
| 19. G. W. Clark | 73. R. A. Vandermeer |
| 20. J. F. Clarke | 74. P. R. Vanstrum (Y-12) |
| 21. J. H. Coobs | 75. T. N. Washburn |
| 22. F. L. Culler | 76. J. R. Weir |
| 23. J. E. Cunningham | 77. W. J. Wilcox, Jr. |
| 24. R. G. Donnelly | 78. M. K. Wilkinson |
| 25. K. Farrell | 79. C. E. Winters |
| 26. J. S. Faulkner | 80. W. J. Yaggi (Y-12) |
| 27. R. J. Gray | 81. H. L. Yakel, Jr. |
| 28. W. O. Harms | 82. F. W. Young, Jr. |
| 29. R. F. Hibbs | 83. A. Zucker |
| 30-34. M. R. Hill | 84. J. H. Frye, Jr. (consultant) |
| 35. P. R. Kasten | 85. W. C. Leslie (consultant) |
| 36. C. C. Koch | 86. John Moteff (consultant) |
| 37. R. S. Livingston | 87. Hayne Palmour III (consultant) |
| 38. A. L. Lotts | 88. J. W. Prados (consultant) |
| 39. T. S. Lundy | 89. N. E. Promisel (consultant) |
| 40. W. R. Martin | 90. G. V. Smith (consultant) |
| | 91. D. F. Stein (consultant) |

EXTERNAL DISTRIBUTION

92. USERDA DIVISION OF CONTROLLED THERMONUCLEAR RESEARCH, Washington, DC 20545
K. M. Zwilsky
- 93-97. USERDA DIVISION OF PHYSICAL RESEARCH, Washington, DC 20545
L. C. Ianniello
D. Readay
D. K. Stevens
M. C. Wittels
S. Wolf

98-99. USERDA OAK RIDGE OPERATIONS OFFICE, P.O. Box E, Oak Ridge, TN 37830

Director
Research and Technical Support Division

100-393. USERDA TECHNICAL INFORMATION CENTER, Office of Information Services,
P.O. Box 62, Oak Ridge, TN 37830

Given distribution as shown in TID-4500 under Materials Category
(25 copies - NTIS)